Available online at www.sciencedirect.com
SCIENCE DIRECT®
Geochimica et Cosmochimica Acta 70 (2006) 1040–1058
Geochimica
www.elsevier.com/locate/gca

Experimental aqueous alteration of the Allende meteorite under oxidizing conditions: Constraints on asteroidal alteration

Catherine L. Jones [1], Adrian J. Brearley *

Department of Earth and Planetary Sciences, MSC03-2040, University of New Mexico, Albuquerque, NM 81731, USA

Received 26 January 2005; accepted in revised form 17 November 2005

Abstract

We have performed an experimental study of the aqueous alteration of the Allende CV3 carbonaceous chondrite under highly oxidizing conditions, in order to examine the alteration behavior of Allende's anhydrous mineralogy. The experiments were carried out at temperatures of 100, 150, and 200 °C, for time periods between 7 and 180 days, with water/rock ratios ranging from 1:1 to 9:1. Uncrushed cubes of Allende were used so that the spatial relationships between reactant and product phases could be examined in detail. Scanning electron microscope studies show that in all the experiments, even those of short duration (7 days), soluble salts of Ca and Mg ($CaSO_4$, $CaCO_3$, and $MgSO_4$) precipitated on the sample surface, indicating that these elements are rapidly mobilized during alteration. In addition, iron oxides and hydroxides formed on the sample surfaces. The sulfates, carbonates, and the majority of the iron-bearing secondary minerals are randomly distributed over the surface of samples. In some instances the iron oxides and hydroxides are constrained to the boundaries of altering mineral grains. Transmission electron microscope studies show that the FeO-rich olivine in the interior of the samples has altered to form interlayered serpentine/saponite and Fe-oxyhydroxides. The degree of alteration increases significantly with increasing water/rock ratio, and to a lesser extent with increasing duration of heating. The serpentine/saponite forms both by direct replacement of the olivine in crystallographically oriented intergrowths, and by recrystallization of an amorphous Si-rich phase that precipitates in pore space between the olivine grains. The alteration assemblage bears many similarities to those found in altered carbonaceous chondrites, although in detail there are important differences, which we attribute to (a) the relatively high temperatures of our experiments and (b) comparatively short reaction times compared with the natural examples. In terms of mineral assemblage, our experiments most closely resemble alteration in the CI chondrites, although the degree of alteration of our experiments is much lower. CI chondrites contain serpentine/saponite intergrowths and veins of Ca-sulfate and Ca-carbonate as well as the Fe-oxyhydroxide, ferrihydrite. However, the phyllosilicate phases formed in our experiments are somewhat coarser-grained than the finest phyllosilicate fraction present in CI chondrites, suggesting that alteration of the CI chondrites occurred at lower temperatures. In terms of mineral assemblage, our experiments also appear to come close to matching CR chondrites, although we infer that CR alteration probably occurred at temperatures <100 °C, based on the very fine-grained size of phyllosilicates in CR matrices.

1. Introduction

Carbonaceous chondritic meteorites are complex aggregates of materials that formed in the solar nebula, 4.56 billion years ago, by a variety of processes including evaporation, condensation, and melting. These materials were subsequently accreted together to form asteroidal parent bodies. Chondritic materials have experienced secondary processing and, accordingly, they retain information regarding the conditions under which the alteration took place. One of the most widespread types of alteration that affected chondritic meteorites, especially the CI and CM chondrites, was the interaction between anhydrous minerals that formed in the solar nebula and a hydrous fluid phase. The central role of water in the evolution of these two carbonaceous chondrite groups has long been recognized (e.g. Pisani, 1864; Kvasha, 1948; Mason, 1960;

* Corresponding author. Fax: +1 505 277 8843.
E-mail address: brearley@unm.edu (A.J. Brearley).
[1] Present address: Los Alamos National Laboratory, C-INC, MS J514, Los Alamos, NM 87545, USA.

0016-7037/$ - see front matter © 2005 Elsevier Inc. All rights reserved.
doi:10.1016/j.gca.2005.10.029

DuFresne and Anders, 1962; Kerridge, 1964; Boström and Fredriksson, 1966; Nagy, 1966; Bass, 1971). This aqueous alteration has contributed significantly to the chemical and mineralogical reworking of the original nebular material and has, to varying degrees, overprinted the primary nebular record. Paradoxically, despite the extensive effects of hydrous alteration, the CI and CM chondrites are compositionally the most primitive solar system material available for study in the laboratory. Distinguishing the primary mineralogical characteristics of nebular materials from the effects of subsequent alteration is extremely important, and one of the central goals of meteorite research. Unequivocal identification of features that result from primary nebular processes can help constrain such important aspects of solar nebular conditions and processes as the thermal history, oxygen fugacity, gas:dust ratio, volatile behavior, and isotopic and chemical reservoirs. All these are essential to modeling the earliest stages of the development of our solar system. Similarly, an improved knowledge of the mineralogical and chemical effects of secondary processing on this primary record provides valuable insights into the early geologic evolution of asteroids.

Although considerable progress has been made in unraveling the complex effects of aqueous alteration in the carbonaceous chondrites based on mineralogical and isotopic studies (Clayton and Mayeda, 1984; Zolensky and McSween, 1988; Brearley, 2003), there are many first order questions which remain either unresolved or controversial. These questions include the location and duration of alteration, the amount, source, and composition of fluid available during alteration, and the physicochemical conditions of alteration. In the latter case, the presence of a particular mineral assemblage or texture should, theoretically, help constrain the temperature and water/rock ratio during alteration, and perhaps the length of time that a given set of conditions prevailed. However, in order to interpret textural and mineralogical information accurately, we require a detailed understanding of the rates and mechanisms of the reactions involved, and how they are impacted by environmental conditions (e.g., temperature, fO_2, pH, etc.). Unfortunately, at present this is generally not possible because the alteration reactions are poorly defined, and very few relevant experimental data are available. The rates and mechanisms of the reactions are known only from terrestrial analogues and end-member experiments, and it is not clear how applicable these data are to meteoritic systems.

As a first step towards improving our understanding of the mechanisms and kinetics of low temperature alteration reactions that have affected the carbonaceous chondrites, we have undertaken a series of hydrothermal experiments using samples of the Allende CV chondrite as a starting material. The experiments have been carried out under highly oxidizing conditions and temperatures between 100, 150, and 200 °C, conditions that are at the extreme end of estimated conditions of alteration for the carbonaceous chondrites (e.g., Zolensky and McSween, 1988; Zolensky et al., 1993). A similar approach has also been used by Tomeoka and Kojima (1995a,b) and Kojima and Tomeoka (1999, 2000) using Allende as a starting material. However, their experiments were performed at a significantly higher temperature (450 °C) and pressure (800 bars) conditions and hence the degree of alteration observed is much higher than observed in the work described here. Our lower temperature experiments have enabled us to observe the very earliest stages of this alteration process, under conditions which more closely approach those experienced by carbonaceous chondrites. We report here the mechanisms and relative rates of the dominant reactions of aqueous alteration, as well as the effects of temperature, water/rock ratio and duration of heating on those rates and mechanisms. The preliminary results of these experiments have been reported in Brearley and Duke (1998), Duke and Brearley (1998a,b) and Jones (2000).

1.1. Starting materials

For this study, we chose to use uncrushed samples of the Allende meteorite as a starting material for our experiments. Allende is a member of the oxidized group of the CV3 carbonaceous chondrites (McSween, 1977; Krot et al., 1995) that has been extensively studied since its fall in 1969. Allende consists of chondrules (43 vol %), calcium–aluminum-rich inclusions (CAIs) (9.4 vol %), amoeboid olivine inclusions (3.2 vol %), lithic and mineral fragments (2.9 vol %), matrix (38.4 vol %), and opaque minerals (3.1 vol %) (McSween, 1977). We chose Allende because it is widely available, has been studied extensively and, consequently, has an extremely well-characterized mineralogy. In addition, it has a mineralogy which is essentially completely anhydrous, with the exception of rare hydrous phases (Wark and Lovering, 1977; Tomeoka and Buseck, 1982a,b; Hashimoto and Grossman, 1987; Keller and Buseck, 1991; Brearley, 1997) that are restricted to chondrules and CAIs. The absence of significant hydrous preterrestrial alteration is important, because it enables differentiation between alteration effects that are of preterrestrial origin and those produced during our experiments. However, we note here that despite the lack of hydrous phases, Allende is not a pristine chondrite, but has experienced considerable secondary alteration that has modified the primary mineralogy in a number of ways (see Krot et al., 1995; Brearley, 2003, for recent reviews). These include: (1) Fe-alkali-halogen metasomatism of CAIs, chondrules and matrix, (2) formation of ferrous olivine rims on chondrules, isolated olivine grains etc., (3) oxidation of sulfidization of opaque assemblages in CAIs, chondrules and matrix, (4) formation of phyllosilicates (discussed above), and (5) formation of platy olivines, Ca–Fe pyroxenes and andradite in the matrix and the formation of pure fayalite.

Our experiments do not replicate alteration of the most primitive chondrites, such as ALH77307 and Acfer 094,

that contain a significant component of amorphous material. Instead, our experiments are intended to establish the general alteration behavior of chondritic materials in the presence of aqueous fluids.

In this study, we concentrated on examining the alteration of the matrix of Allende, because this material is fine-grained and is most susceptible to alteration by aqueous fluids. Allende matrix is composed predominantly of fayalitic olivine, with numerous other minor phases including clinopyroxene (diopside–hedenbergite (Di–Hd) solid solutions), magnetite, pyrrhotite, pentlandite, andradite, wollastonite, nepheline, sodalite, Ca-phosphate, kirschteinite, and awaruite (Ni_3Fe) (Peck, 1983; Scott et al., 1988; Toriumi, 1989; Krot et al., 1995). The fayalitic olivine ($\sim Fa_{45–56}$; Peck, 1983) occurs in two forms; elongate laths 8–25 μm long and 1–3 μm thick, and anhedral grains ~1–3 μm in size (Peck, 1983). The laths are more abundant than the anhedral grains. Pentlandite, chromite, and poorly graphitized carbon are present as nanometer-sized inclusions in matrix olivine grains (Brearley, 1999). No phyllosilicates or other hydrous phases have been reported in Allende matrix. For a detailed description of the mineralogy of other components of Allende see Brearley and Jones (1998) and references therein.

1.2. Experimental methods

Cubes, approximately 3 mm on a side, were cut from a sample of Allende from the University of New Mexico collection and were placed in Teflon-lined acid digestion bombs (Parr bombs). Aliquots of 18 MΩ deionized water were added to provide initial water/rock ratios of between 1:1 and 9:1 by volume. The samples were heated in a Lindberg/Blue oven to between 100 and 200 °C, for periods ranging between 7 and 180 days (conditions are summarized in Table 1). The Teflon reaction vessels are 23 mL, a volume much larger than that of the meteorite cubes and the samples were loaded in air so the initial oxygen fugacity of the experimental environment was considered to be atmospheric. At 200 °C if water is present in both liquid and vapor phases, the pressure is ~15.5 bars (Haar et al., 1984). It is possible in the lower water experiments that all the water was in the vapor phase. Assuming that water acted as an ideal gas, the pressure at an initial water/rock ratio of 1:1 to would be on the order of 10 bars. At higher water/rock ratios enough liquid water was present to ensure that both phases coexisted so we estimate that experimental pressures may perhaps have been as low as 10 bars but did not exceed 15.5 bars.

Table 1
Summary of experimental conditions, and characteristic of the predominant alteration phases precipitated on the sample surfaces under oxidizing conditions

Temperature (°C)	Heating duration (days)	Water/rock ratio	Dominant phases formed	Morphology	Grain size	Weight gained (%)
200	7	1:1	$CaSO_4$	Hexagonal prisms	~10 × 100 μm	3.1
200	7	2:1	$CaSO_4$	Tabular	~20 μm	2.7
			$MgSO_4$	Fuzzy; Cracked	sub-micron	
200	14	1:1	$CaSO_4$	Tabular	~100 μm	3.1
200	21	1:1	$CaSO_4$	Strands	~50 μm	2.9
			$CaCO_3$	Rhombs	30–50 μm	
200	30	1:1	$CaSO_4$	Hexagonal prisms	~50 × 100 μm	2.4
200	30	2:1	$CaCO_3$	Complex twins	~20 μm	3.0
			Fe-(hydro)oxide	Spherules	sub-micron	
200	30	3:1	$CaSO_4$	Tabular	20–100 μm	5.5
200	60	1:1	$CaSO_4$	Hexagonal prisms	~200 μm	2.4
			Fe-(hydro)oxide	Acicular	sub-micron	
200	60	2:1	$CaSO_4$	Twinned rhombs	~150 μm	3.6
			$MgSO_4$	Fuzzy; Cracked	sub-micron	
200	60	3:1	$CaSO_4$	Tabular	100 × 200 μm	Unknown
200	90	2:1	$CaCO_3$	Rhombohedral	~100–200 μm	3.4
200	90	9:1	$CaCO_3$	Rhombohedral	50–100 μm	2.6
			$CaSO_4$	Laths	1 mm	
			Fe-(hydro)oxide	Friable	sub-micron	
150	60	1:1	$CaSO_4$	Hexagonal prisms	~200 μm	2.1
			Fe-(hydro)oxide	Spherular	sub-micron	
150	60	3:1	$CaCO_3$	Interlocking rhombs	~3–4 μm	1.5
150	60	6:1	$CaSO_4$	Laths	~200 μm	2.1
			$CaCO_3$	Anhedral	~50–100 μm	
100	180	1:1	$CaSO_4$	Laths	~50 μm	N/A
			$CaCO_3$	Orthorhombic	~10 × 20 μm	
100	180	2:1	$CaSO_4$	Blocky	~50 μm	1.9
			Fe-(hydro)oxide	Lacy		

After heating, product phases that precipitated on the sample exteriors were examined initially using a binocular microscope, and later using a JEOL 5800LV scanning electron microscope (SEM) operating in low vacuum mode. More quantitative analyses were made on carbon-coated, but still uncut, samples using energy dispersive X-ray spectroscopy (EDS) on the same SEM. An Oxford Link ISIS 200 analytical system fitted with a Pentafet ultrathin window X-ray detector was used for the EDS analyses.

Demountable, doubly polished thin sections were prepared from the experimental samples and were studied by analytical SEM in order to examine alteration effects in the interior of the samples. We concentrated on searching for any alteration effects in the matrix of the altered Allende samples, because we anticipated that alteration of this material would be most rapid given its fine grain size and high surface area. Selected areas of material were then removed from the thin sections and ion milled using a Gatan model 600 dual ion mill. Subsequently, samples were analyzed on a JEOL 2010 high-resolution transmission electron microscope (HRTEM) operating at 200 kV. Quantitative compositional data were obtained using an Oxford ISIS EDS system with an ultra-thin window Oxford Pentafet detector. Data reduction were carried out using the Cliff-Lorimer thin film approximation, and experimental *k*-factors, determined from a variety of standards, were used.

The modeling program Geochemist's Workbench 3.0 was used to plot relevant activity–activity diagrams at 200 °C.

2. Results

After the experiments, all the samples had developed a reddish-brown coloration on their surfaces, irrespective of run duration or initial water content. SEM studies of the altered samples showed that a variety of alteration phases have crystallized on the surface of each cube. Compositionally, these phases are predominantly Ca-sulfate, Ca-carbonate, and Fe-oxides or hydroxides which were identified by qualitative energy-dispersive X-ray spectroscopy (EDS). Each of these phases occurs in a variety of different morphologies. The degree to which each sample is altered depends on the temperature and duration of heating, as well as the initial water/rock ratio of the experiment. The majority of the alteration phases are distributed randomly on the surface of the samples without regard to substrate. However, in several samples, growth of new phases is locally constrained to the exposed surfaces of particular phases. These features are summarized in Table 1, and described in more detail below.

Transmission electron microscope (TEM) studies of the material in the interior of the samples show that phyllosilicates, iron oxides or hydroxides, and an amorphous silica phase are the predominant alteration phases. The characteristics of these phases, such as their grain sizes, degree of crystallinity, and relative abundances change as a function of reaction progress.

2.1. Alteration on the sample surfaces: SEM analyses

Our SEM observations of the alteration products that formed on the surface of the uncut sample cubes are summarized below. The results are presented in three main groups of samples that were heated to 200, 150, and 100 °C, respectively. For brevity only the key observations are presented below. For a detailed description of the experimental products see Jones (2000).

2.1.1. Experiments carried out at 200 °C

At 200 °C, we ran samples for periods of 7, 14, 21, 30, 60, and 90 days at water/rock ratios that range from 1:1 to 8:1 (Table 1). In all these samples, alteration phases have formed on the surface of the cube. For a given water/rock ratio, the abundance of these phases increases as function of reaction time and systematic increases in grain size are observed. The main alteration products are Ca-sulfate and Ca-carbonate that occur distributed randomly on the surface of the sample, without regard to substrate and with no apparent orientation relationships. We refer to these phases as $CaSO_4$ and $CaCO_3$, below. We do not know the degree of hydration of the $CaSO_4$, although we have some morphological evidence (see below) that it changes in some experiments as a function of time. Fe-oxides and hydroxides are also commonly formed and, in rare examples, we have observed $MgSO_4$.

The most common alteration phase present in all the samples is $CaSO_4$, and may include gypsum, bassanite, and anhydrite. The $CaSO_4$ occurs with and without $CaCO_3$, and in a variety of morphologies including euhedral, hexagonal prisms, approximately 5–10 μm in diameter and 50–100 μm in length (Fig. 1A), and tabular crystals that sometimes occur as aggregates (Figs. 1B and C). Our data suggest that these morphological differences are a reflection of the water/rock ratio of the experiments. For example, we typically find hexagonal prisms in experiments run with water/rock ratios of 1:1 (e.g., Fig. 1A) and tabular morphologies when the water/rock ratio is increased to 3:1, irrespective of run time. We interpret this change in morphology as reflecting the degree of hydration of the $CaSO_4$. The hemihydrate of $CaSO_4$, bassanite, is monoclinic and pseudo-hexagonal, and gypsum ($CaSO_4{\cdot}2H_2O$), while also monoclinic, often favors a tabular habit (Klein and Hurlbut, 1993).

The correlation between run duration and grain size for $CaSO_4$ is well illustrated by a series of experiments, run at water/rock ratios of 1:1 and 3:1. Hexagonal prisms in the 1:1 experiments increase from ~10 μm in diameter and 100 μm long after 7 days, to ~50 μm wide and ~100 μm long after 30 days and finally to ~200 μm long after 60 days. A similar progression in size is evident in the more tabular grains formed in the 3:1 experiments, with those formed in the 30-day experiment being 20–100 μm wide, increasing in width up to 200 μm in the 60-day experiment. The largest grain sizes occur in an experiment run for 90 days at very high water/rock ratio (9:1) where laths of

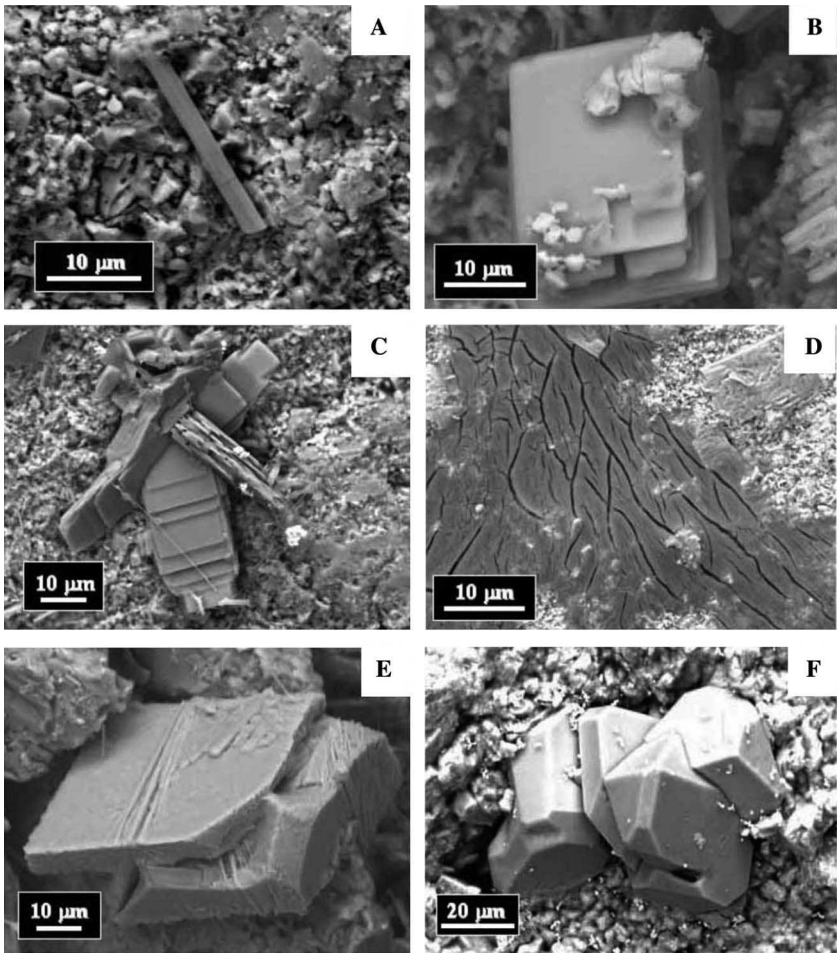

Fig. 1. Back-scattered electron micrographs of morphological characteristics of sulfates and carbonates on the surfaces of cubes of Allende after the experimental runs. (A) Hexagonal prism of $CaSO_4$ on sample surface (200 °C, 7 days, w/r = 1:1). (B) Single tabular crystal of $CaSO_4$ precipitated on the sample surface (200 °C, 7 days, w/r = 2:1). (C) Tabular aggregate of $CaSO_4$ crystals (200 °C, 14 days, w/r = 1:1). (D) $MgSO_4$ forming as a cracked coating and as a light "fuzzy" phase on the sample surface (200 °C, 7 days, w/r = 2:1). (E) Stranded overgrowths of $CaSO_4$ on a $CaCO_3$ grain (200 °C, 21 days, w/r = 1:1). (F) Complexly twinned calcite crystals (200 °C, 30 days, w/r = 2:1).

$CaSO_4$ up to 1 mm in size have precipitated. We have only observed one case where the formation of $CaSO_4$ is clearly related to the substrate. In this sample (60 days, w/r 2:1), a melilite grain, presumably in an exposed CAI, has altered to numerous small (2×10 μm) $CaSO_4$ laths that are spatially restricted to the surface of the melilite grain. The other sulfate produced in these experiments is $MgSO_4$ which occurs as a cracked coating on the surface of only one sample (60 days, w/r 2:1; Fig. 1D).

$CaCO_3$ is present in some, but not all of the samples (see Table 1). It too occurs in a variety of morphologies, including individual grains and complex aggregates of rhombohedral and twinned crystals (Figs. 1E and F). It is usually present as a subordinate phase to $CaSO_4$, but in rare samples is the dominant phase (Table 1). Grain sizes can range up to ~200 μm in longer duration experiments (90 days). In some experiments, we have observed $CaSO_4$ overgrowing $CaCO_3$ crystals in irregular, stranded overgrowths (Fig. 1E), suggesting that the $CaCO_3$ precipitated first and was later overgrown by Ca-sulfate.

Fe-(hydro)oxides are ubiquitous on the surfaces of all the samples. Two distinct Fe-oxide or hydroxide phases are present. One is acicular and extremely fine-grained and covers the exposed matrix (Fig. 2A), but is not found on the surfaces of exposed chondrules. This is probably the phase responsible for the reddish discoloration of the sample surface. The second phase occurs as submicron spherules that form loose aggregates. They are randomly distributed without regard to sample substrate, and are often associated with the $CaCO_3$ grains and with a lacy material (Fig. 2B). In some experiments, the $CaCO_3$ and the $CaSO_4$, as well as the sample surface, are covered in abundant, friable, submicron Fe-(hydro)oxide.

In some samples (e.g., 60 days, 1:1 and 2:1 water/rock), we observed evidence of direct alteration of individual grains exposed on the cube surface. In the 1:1 sample, pentlandite and pyrrhotite grains are altered to secondary phases that are restricted to the surface of the grains rather than being randomly distributed across the surface of the cube.

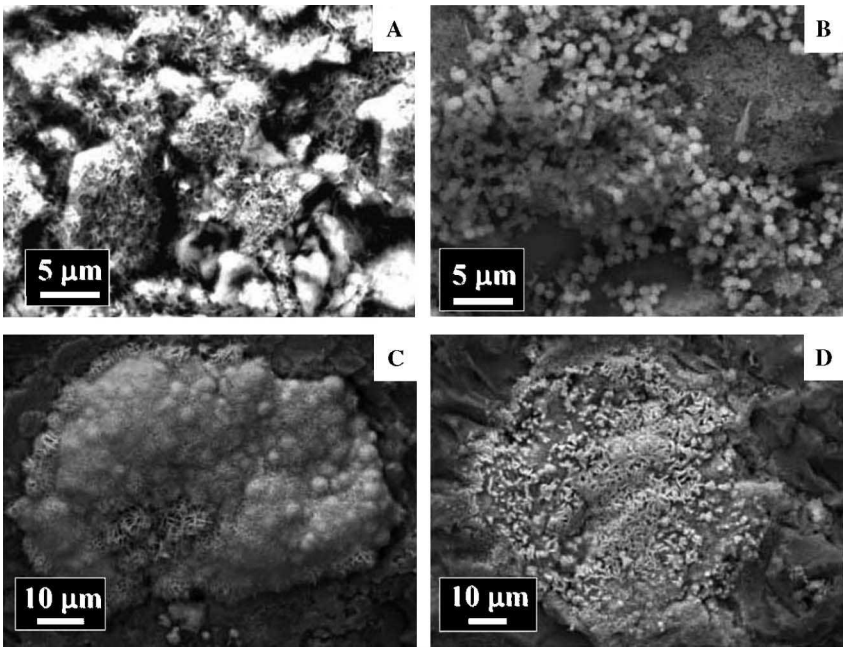

Fig. 2. Backscattered electron micrographs of Fe-oxyhydroxides and sulfides on the cube surfaces after the experimental runs. (A) BSE image of extremely fine-grained Fe-(hydro)oxide (200 °C, 30 days, w/r = 2:1) distributed over the surface of matrix olivine grains. (B) Spherular Fe-(hydro)oxide phase (200 °C, 30 days, w/r = 2:1) on the surface of the cube. (C) Ni-sulfide growing on a matrix pentlandite grain exposed at the surface (200 °C, 60 days, w/r = 1:1). The new sulfide is restricted to the size of the pentlandite grain. (D) Fe-(hydro)oxide growing on a matrix pyrrhotite grain exposed at the surface (200 °C, 60 days, w/r = 1:1).

The pentlandite has altered to a very fine-grained Ni- and S-rich phase that consists of submicron acicular crystals (Fig. 2C). The pyrrhotite alteration product is an Fe-(hydro)oxide that occurs as tiny (<1 μm) particles with a variety of acicular and irregular habits (Fig. 2D).

2.1.2. Experiments carried out at 150 °C

Three experiments were carried out for 60 days at 150 °C with water/rock ratios of 1:1, 3:1, and 6:1. In the 1:1 experiment, $CaSO_4$ forms elongate (~200 μm) hexagonal prisms similar to those observed in the 200 °C experiments, but are more complexly twinned and less euhedral. In the 6:1 experiments, the $CaSO_4$ occurs as laths. $CaCO_3$ is the only alteration phase present in the 3:1 sample and occurs as tiny (3–4 μm), interlocking rhombs that cover the surface of the cube. $CaCO_3$ also occurs along with $CaSO_4$ in the 6:1 experiment. Fe-(hydro)oxide occurs as sub-micron spherules and as a very thin film that overlies the surface of the cubes as well as the $CaSO_4$ crystals.

2.1.3. Experiments carried out at 100 °C

Two experiments lasting 180 days were performed at 100 °C. $CaSO_4$ has precipitated as rectangular laths (water/rock ratio 1:1) and anhedral grains (water/rock ratio 2:1) and $CaCO_3$ has also precipitated as 10×20 μm grains that are extremely beam sensitive. Fe-(hydro)oxide occurs in both samples; as sparsely distributed 1–2 μm grains with irregular morphologies in the 1:1 sample, and as a lacy covering in the 2:1 sample.

2.2. Alteration of sample interiors: TEM analyses

A number of samples, covering a range of conditions, were selected for study by TEM. These studies were aimed at obtaining detailed information on the alteration behavior of the matrix in the interior of the cubes.

TEM observations of a sample heated at 200 °C for 30 days (1:1 water/rock ratio) show that the matrix olivine has altered extensively to phyllosilicates, iron oxides or hydroxides, and a silica-rich amorphous phase that contains up to 60 wt% SiO_2 with FeO, MgO, and Al_2O_3 as other major elements. The most common alteration phase in this sample consists of very fine-grained, phyllosilicate crystals that form on the (010) faces of the altering olivine grains (Fig. 3A). These phyllosilicates are approximately 50–60 nm long and 10 unit cells wide and form subparallel structures on the surface of the olivine (Fig. 3B). High resolution TEM imaging shows that the phyllosilicates are intimate intergrowths of two phases, one with a basal spacing of ~0.7 nm, and the other with a more variable basal spacing that is usually close to 1.0 nm but can range as high as 1.4 nm (Fig. 3B). We interpret these phases as being serpentine (0.7 nm) and saponite (1.0–1.4 nm), respectively. Saponite is known to have variable basal spacings depending on its degree of hydration (Deer et al., 1966; Brearley, 1995) and may also undergo dehydration in the electron beam during analysis (Klimentidis and Mackinnon, 1986; Tomeoka and Buseck, 1988).

The growth of the phyllosilicates is clearly crystallographically controlled by the structure of the olivine, with

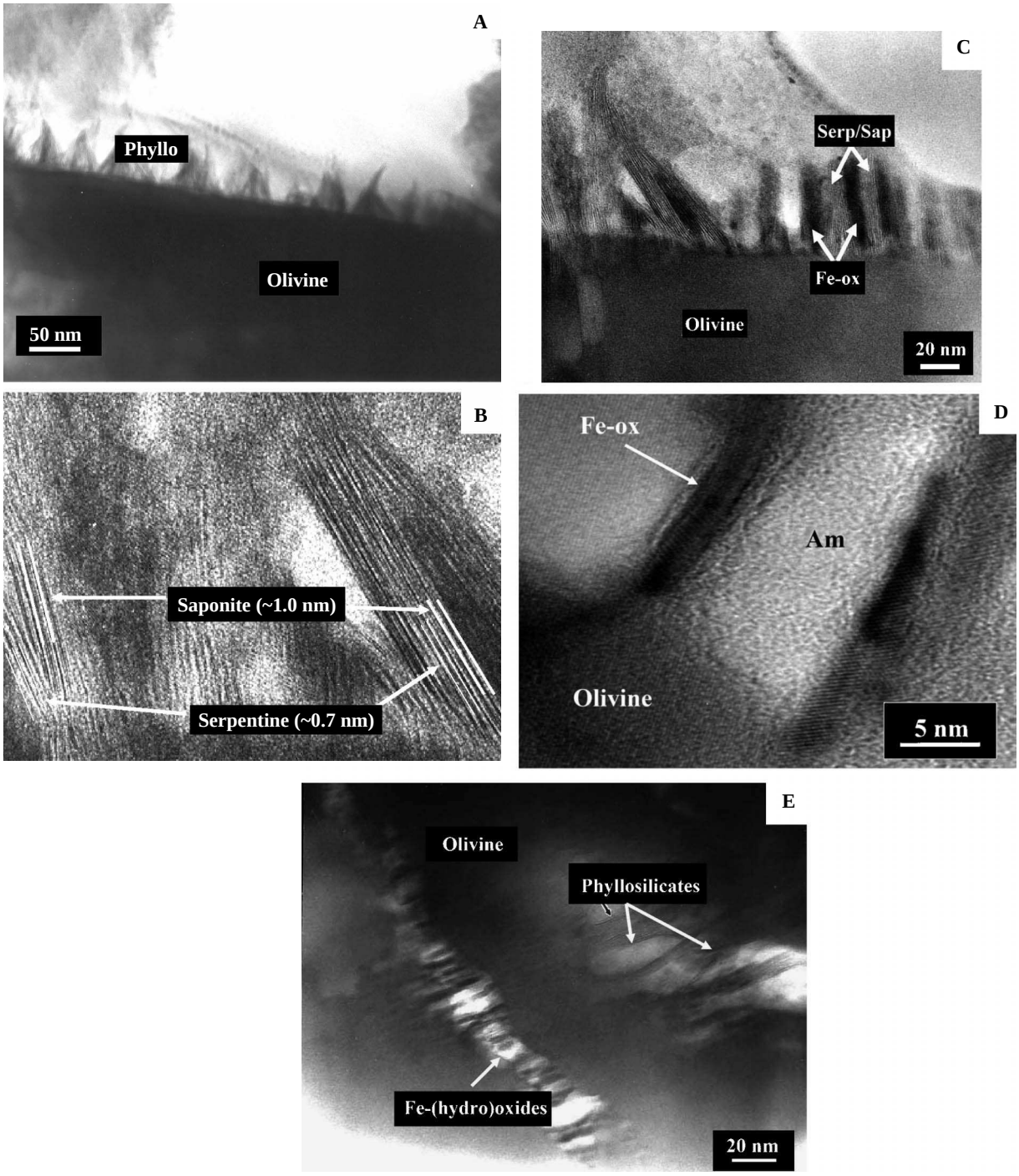

Fig. 3. Transmission electron micrographs showing the alteration textures in the matrix of the altered Allende samples in an experiment run at 200 °C, 30 days, w/r = 1:1. (A) Bright field TEM image showing sub-parallel aggregates of phyllosilicates that have nucleated and are growing on the (010) face of an altering matrix olivine grain. (B) High resolution TEM image of the phyllosilicate aggregates in (A) showing that they consist of sub-parallel phyllosilicates with interlayering of two phases, serpentine (~0.7 nm) and saponite (~1.0 nm). (C) HRTEM image of cellular texture formed by serpentine/saponite and Fe-(hydro)oxides during the alteration of olivine. (D) HRTEM image showing tiny Fe-(hydro)oxide crystals fingering out from the altering olivine into an amorphous phase. (E) TEM image of oriented phyllosilicate and Fe-(hydro)oxide crystals within fractures and pore spaces inside an altering olivine grain.

the *c*-axis of the serpentine parallel to the altering olivine (010) face. In some cases, microcrystalline Fe-(hydro)oxides are intimately intergrown with the serpentine and saponite, forming a cellular texture (alternating dark and light bands in Fig. 3C). At some reacting olivine surfaces, sub-parallel, elongate Fe-(hydro)oxide crystals, approximately 20 nm long and 2–3 nm wide, finger out from the olivine surface into the amorphous phase (Fig. 3D). Oriented precipitates of both the phyllosilicate and the Fe-(hydro)oxide phases also occur within fractures and pore spaces inside

Table 2
d-Spacings of Fe-(hydro)oxide phases in the sample heated to 200 °C for 30 days at an initial water/rock ratio of 1:1

$d_{measured}$	Magnetite PDF #19-0629		Maghemite PDF #24-0081		Akaganeite PDF #08-0093	
	$d_{calculated}$	(hkl)	$d_{calculated}$	(hkl)	$d_{calculated}$	(hkl)
4.73	4.85	(111)	4.82	(111)	4.70	(120)
4.11	4.19	(200)	4.18	(200)	n.m.	n.m.
3.69	3.75	(210)	3.73	(210)	3.68	(220)
3.50	3.43	(211)	3.41	(211)	3.52	(030)
3.00	n.m.	n.m.	n.m.	n.m.	3.04	(001)
2.95	2.97	(220)	2.95	(220)	2.92	(011)
2.91	n.m.	n.m.	n.m.	n.m.	2.91	(101)
2.75	2.79	(300)	2.78	(300), (221)	n.m.	n.m.
2.71	n.m.	n.m.	n.m.	n.m.	n.m.	n.m.
2.61	2.63	(310)	2.64	(310)	2.62	(201)
2.59	n.m.	n.m.	n.m.	n.m.	n.m.	n.m.
2.56	2.53	(311)	2.52	(311)	2.56	(140)
2.34	2.33	(320)	2.32	(320)	2.28	(301)
2.14	2.10	(400)	2.09	(400)	2.12	(050)

n.m., no matching *d*-space.

the olivine grains (Fig. 3E). We obtained *d*-spacings for the Fe-oxide or hydroxide phase(s) in this sample by Fast Fourier Transform (FFT) processing of digital high resolution TEM images (Table 2). These *d*-spacings match best with either maghemite (γ-Fe_2O_3), or magnetite (Fe_3O_4) and to a lesser degree with akaganéite (β-FeO(OH)) (Table 2).

An amorphous, silica-rich phase has precipitated along the olivine grain boundaries and within the interstices between the matrix olivine grains. Tiny phyllosilicate crystallites, 10–20 nm long and only 2–3 unit cells wide, have nucleated within this amorphous phase.

To examine a sample that was altered under extreme conditions, we studied a second sample that was heated to 200 °C for 90 days with an initial water/rock ratio of 9:1. Alteration in this sample has progressed much further as shown in Fig. 4A, an overview of the altered matrix in which extensive development of phyllosilicates is apparent. Phyllosilicates dominate the alteration assemblage in this sample and secondary Fe-(hydro)oxide phases are rare. Matrix olivine crystals have altered preferentially along (010) faces, and crystallographically oriented phyllosilicate crystals have developed as overgrowths on the altering olivine. Randomly oriented phyllosilicates also occur in the interstices between olivine grains, probably due to recrystallization of the amorphous silica phase, which appears to be rarer in this sample. High resolution TEM imaging shows that the phyllosilicates are complex unit cell intergrowths of serpentine and saponite, as in the experiment carried out at 200 °C, for 30 days (w/r 1:1). Grains that consist predominantly of serpentine with few saponite interlayers (e.g., Fig. 4B) have a planar morphology, although larger crystals can show waviness and curvature, suggesting that the dominant serpentine polymorph present is lizardite. The absence of any concentric structures in our samples indicates that no chrysotile has been formed

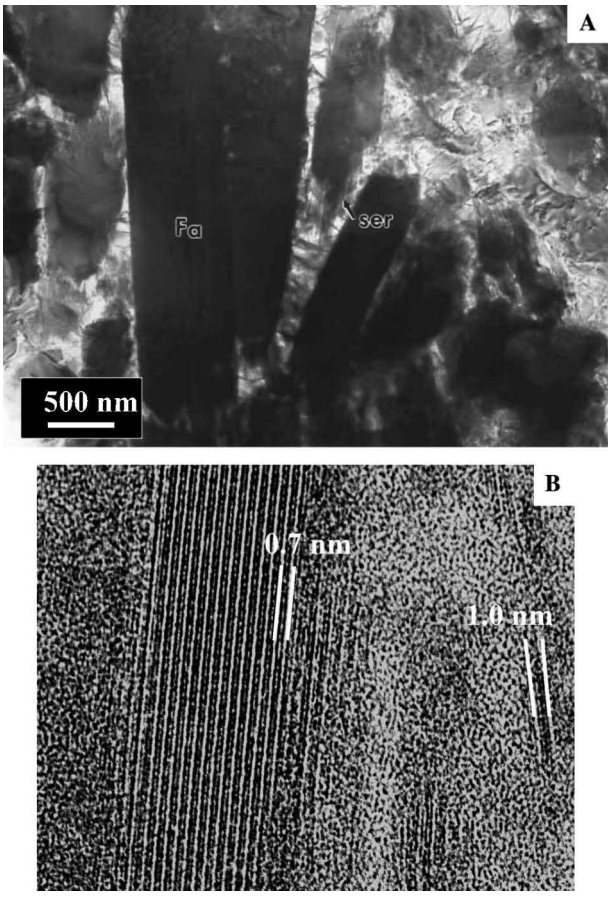

Fig. 4. (A) Low magnification TEM image of alteration of olivine in the matrix of an Allende sample run at 200 °C, 90 days, w/r = 9:1. The interstices between the olivine grains are filled with phyllosilicate grains, many of which have formed as oriented overgrowths parallel to the *c*-axis of the olivine grains (arrowed). (B) HRTEM image of a serpentine grain from the same sample as Fig. 5A showing the 0.7 nm basal spacing. Note the 1.0 nm basal spacing of one of the layers in this grain, as well as of the isolated layer in the lower right corner.

in the alteration reactions. Further, the modulated structures characteristic of antigorite are also absent.

Serpentine/saponite intergrowths are found in two distinct occurrences in this sample. First, they occur as parallel to subparallel crystallites that are associated with the preferential alteration of the (010) face of olivine grains (Fig. 5A). There is a distinct orientation relationship between the olivine and the replacing serpentine and saponite, i.e., $c_{serp/sap}//a_{ol}$ (Fig. 5A). The full-orientation relationship could not be obtained due to strong streaking in the diffraction rows caused by the intergrowth of the two phyllosilicate phases. The serpentine and saponite are very fine-grained (~20–30 unit cells wide) to a distance of ~50 nm away from the olivine grain, where a distinct change in grain size occurs (Fig. 5B). The phyllosilicates remain parallel to subparallel, but are much coarser-grained, forming long ribbons that extend for 100 s of nm and are up to 50 nm wide. The predominant morphology of grains is platy although they become more curved and wavy further from the olivine grain.

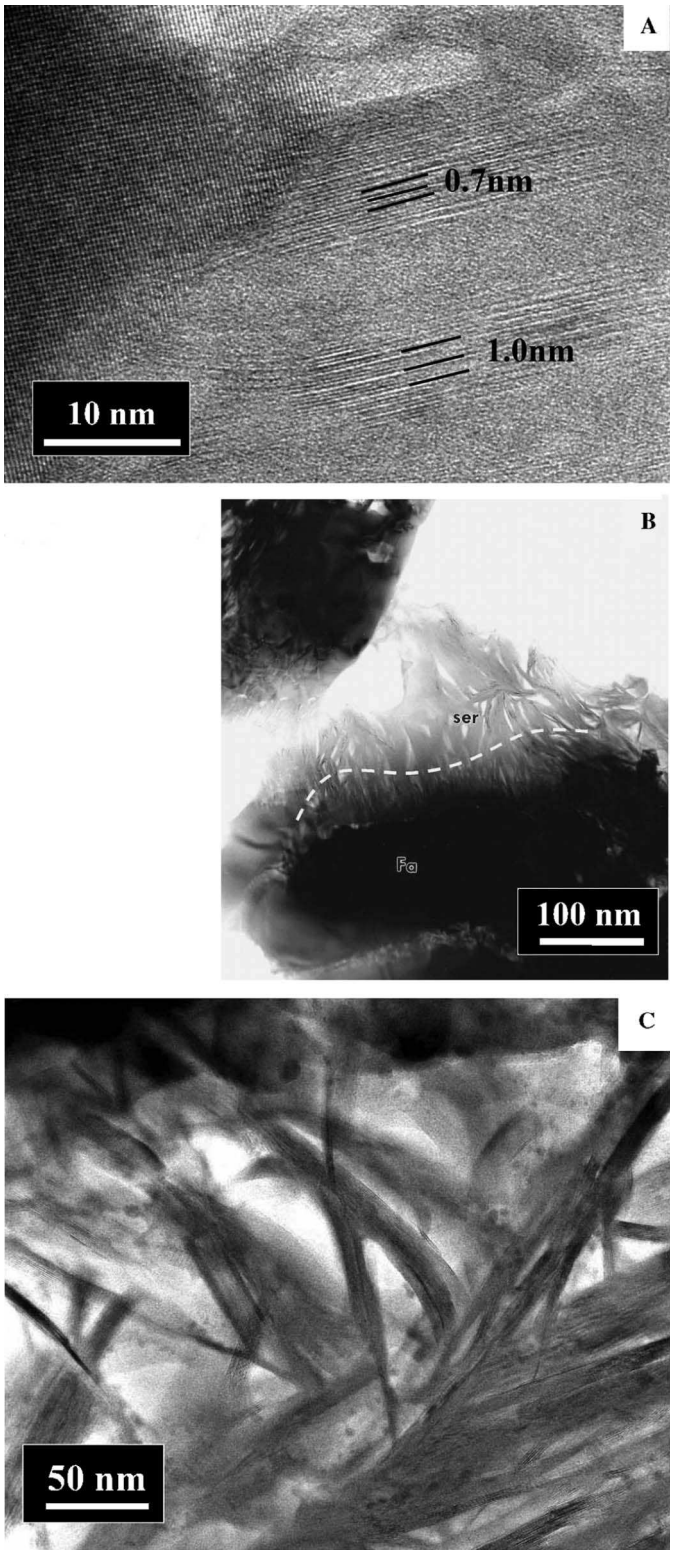

Fig. 5. Transmission electron micrographs of the relationships between serpentine/saponite intergrowths and altering olivine grains (200 °C, 90 days, 9:1). (A) HRTEM image of the (010) face of an olivine grain altering to saponite (1.0 nm) and serpentine (0.7 nm). (B) Bright field image showing recrystallization front in the serpentine. The phyllosilicates are fine-grained in a layer immediately adjacent to the reacting olivine. Beyond the dashed line the serpentine grains are coarser and form long ribbons that extend into the interstitial space between the olivine grains. (C) Randomly oriented serpentine/saponite that has probably crystallized from the amorphous silica-rich phase in the interstices between the matrix olivine grains.

The second type of serpentine/saponite intergrowth is randomly oriented and the grains have curved and wavy morphologies (Fig. 5C). These intergrowths have nucleated and grown in the amorphous silica phase in the interstices between matrix olivine grains, and individual crystals often appear to be set in a matrix of the amorphous material. The individual grains within these random arrays are relatively fine-grained, only ~10 nm in width, although they can be as much as 100 nm in length. There is no evidence that the growth of these phyllosilicates is crystallographically controlled by the altering olivine.

Analytical electron microscopy (AEM) was used to study the composition of the phyllosilicate alteration products from the sample heated to 200 °C for 90 days at an initial water/rock ratio of 9:1. Analyses of the phyllosilicates are plotted on an atom % Fe–Mg–Si+Al ternary diagram in Fig. 6 and representative EDS analyses are reported in Table 3. The phyllosilicate compositions straddle the

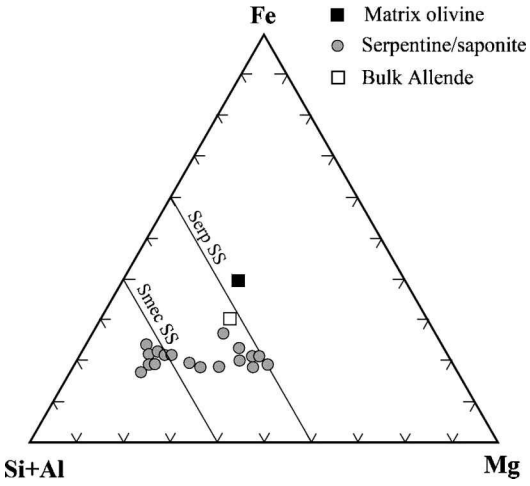

Fig. 6. Fe–Mg–Si + Al atom% ternary diagram showing phyllosilicate compositions from a sample heated at 200 °C for 90 days at an initial water/rock ratio of 9:1.

Table 3
Analytical electron microscope analyses from representative phyllosilicates in a sample heated to 200 °C for 90 days at an initial water/rock ratio of 9:1

Element	Atom wt%							
Na	2.72	1.08	1.27	n.d.	n.d.	n.d.	n.d.	n.d.
Mg	14.88	10.49	9.37	11.30	7.71	7.37	6.46	5.19
Al	2.33	1.96	2.04	1.95	5.63	8.28	4.90	6.95
Si	14.72	19.08	19.57	16.53	17.15	15.46	18.78	17.58
S	n.d.	n.d.	n.d.	0.08	0.38	0.11	0.10	0.06
K	0.16	0.05	0.03	n.m.	0.08	0.07	0.15	0.05
Ca	0.08	0.02	0.01	0.14	0.25	0.09	0.16	0.01
Ti	0.01	0.01	n.d.	n.d.	n.d.	n.d.	n.d.	n.d.
Mn	0.22	0.13	0.05	0.10	0.09	0.06	0.08	0.10
Fe	7.52	7.33	7.51	11.15	8.23	8.53	8.57	9.31
Ni	n.d.	n.d.	n.d.	0.05	n.d.	0.05	n.d.	n.d.
Fe/(Fe + Mg)	0.33	0.41	0.44	0.50	0.52	0.54	0.57	0.64

n.d., not detected.

smectite solid solution line and extend in a linear array towards the serpentine solid solution line, consistent with intergrowths of smectite and serpentine that are too finely intergrown to be resolved by the electron beam. Some of the smectite data lie off the smectite solid solution line, closer to the Si+Al-rich apex, an effect which we attribute to beam overlap with the Si-rich amorphous material in which the phyllosilicates are embedded.

The Fe/(Fe + Mg) ratio of these phyllosilicates varies between 0.33 and 0.64 with an average value of 0.45. The EDS analyses also show that they are relatively Fe- and Al-rich (Table 3) with an average of 8.31 wt% total iron expressed as Fe^{2+} and 4.18 wt% Al. According to Wicks and Plant (1979), lizardite is the serpentine polymorph that exhibits most significant substitution by Al and Fe, supporting our identification of the serpentine as lizardite, based on its planar morphology.

These AEM data also provide a means of assessing the approximate modal proportions of smectite and serpentine in this sample. The proportions of the two phases appear to vary on a highly localized (submicron) scale, precluding an accurate assessment of the relative abundances of the two phases, using high-resolution TEM images alone. The distribution of the random analytical electron microscope analyses in Fig. 6 suggests that smectite may be slightly more abundant that serpentine. However, a more accurate determination would require a significantly larger dataset than is currently available.

In addition to the above samples, run at 200 °C, we used TEM to study a sample run at 150 °C (60 days, w/r = 1:1). Incipient alteration has occurred both on the surface of the matrix olivine grains and in cracks and pore spaces within the grains. Precipitation of a silica-rich amorphous phase has occurred in the interstices between the matrix olivine grains. Nanocrystalline phyllosilicates, only 10–15 nm long and a few unit cells wide, grow out from the surface of some olivine grains into the amorphous phase (Fig. 7A). Intimately intergrown phyllosilicate and Fe-(hydro)oxide phases form ladder-like textures in fractures within the matrix olivine grains. These fractures are only ~50 nm wide and the phyllosilicates and Fe-(hydro)oxides grow across the gap, normal to the surface of the olivine, as well as laterally along the fracture parallel to the olivine surface (Fig. 7B). These phyllosilicate crystals are only a few unit cells wide, but are the dominant phase present in the intergrowths. High resolution TEM shows that the basal spacing of the phyllosilicate phase is ~0.71 nm, consistent with serpentine.

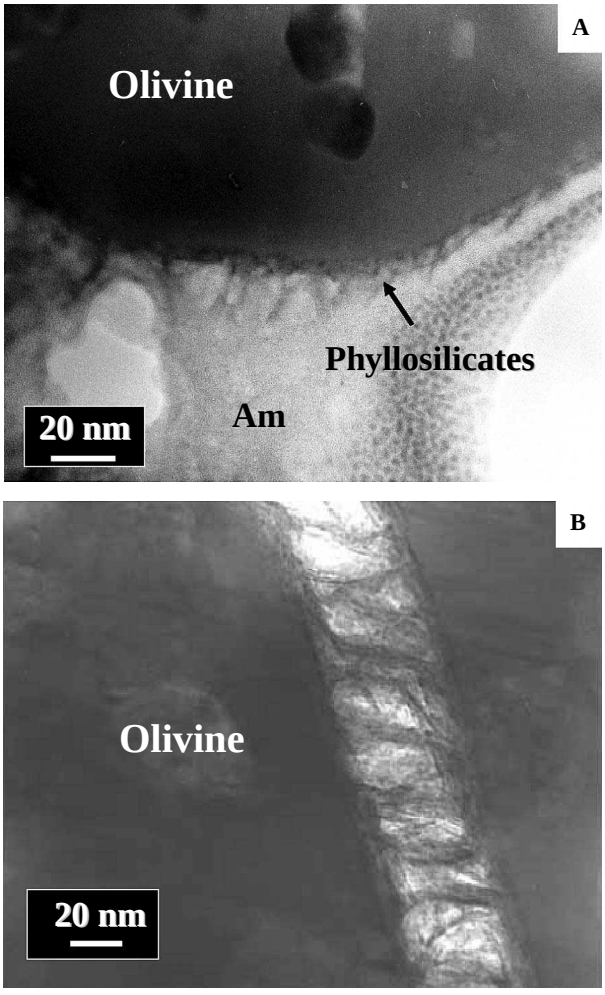

Fig. 7. Transmission electron micrographs of alteration textures from an experiment run at 150 °C, 60 days, w/r = 1:1. (A) Bright field TEM image of protophyllosilicates forming on the surface of an altering olivine. The material further from the olivine is an amorphous Si-rich material (labeled Am). (B) Bright field TEM image of ladder-like serpentine precipitates filling a fracture in a matrix olivine grain.

3. Discussion

3.1. Introduction

As documented above, there is considerable evidence of aqueous alteration in our samples run at temperatures between 100 and 200 °C. SEM analyses of the sample exteriors show that secondary sulfate, carbonate, and Fe-(hydro)oxide minerals have formed on the cube surfaces. None of these phases has ever been described in unaltered Allende samples. These minerals provide insights into the mobility of elements being released by the alteration of minerals in the interior of the samples. The random distribution, without regard to substrate, of Ca-sulfate and Ca-carbonate on the sample surface indicates that these soluble salts are entering the fluid phase and are being transported and precipitated on the surface. In addition to mobilization of soluble ions, TEM analyses demonstrate that extensive reaction has occurred in the sample interiors, enabling the abundance and distribution of the product phases to be studied in detail. In this section, each of the major alteration reactions, along with its mechanisms and relative rates, is discussed in detail.

3.2. Mechanisms of iron-rich olivine alteration

It is clear from our experiments that the dominant alteration reaction involves the oxidation and hydrolysis of the

fine-grained iron-rich olivine (~Fa_{50}) in the matrix of the samples. This reaction may be represented by the general equation:

$$\text{Fe-bearing olivine} + H_2O = \text{Phyllosilicates} + \text{Fe-(hydro)oxide}$$

Based on experiments run for different times, and with a range of water/rock ratios, we have been able to gain insights into the alteration mechanism at different stages from incipient to advanced. In our samples, we observe evidence for this reaction occurring by two distinct pathways, one involving direct replacement of the olivine and a second by a two step process that involves dissolution of olivine followed by reprecipitation of new alteration phases.*3.2.1. Direct transformation mechanism*

The direct alteration of matrix olivine to crystalline serpentine, saponite, and Fe-(hydro)oxide occurs by preferential alteration of the (010) faces of olivine grains. After heating at 200 °C for 30 days with a water/rock ratio of 1:1, the initial alteration of olivine is characterized by clusters of sub-parallel serpentine and saponite intergrowths, 50–60 nm in length, that converge to an apex away from the interface with the olivine (Fig. 3A). Alteration is also evident in the interiors of the olivine grains where oriented precipitates of phyllosilicates and Fe-(hydro)oxides are observed in voids within the parent crystal (Fig. 3E).

In the sample heated at 200 °C for 90 days with an initial water/rock ratio of 9:1, alteration has progressed further. Fine-grained, crystallographically oriented intergrowths of serpentine and saponite extend for ~50 nm from the altering grain (Fig. 5A). The orientation relationship between the serpentine and the altering olivine is $c_{serp/sap}//a_{ol}$. Approximately 50 nm from the altering olivine grain there is a sharp discontinuity in the phyllosilicate grain sizes (Fig. 5B). The serpentine and saponite crystals furthest from the olivine are sub-parallel with their long axes normal to the altering face of the olivine grain, but they are longer and much coarser-grained (up to 50 nm wide and 100 s of nm long). We interpret this feature as a recrystallization front created by the progressive coarsening of the very fine-grained serpentine/saponite formed directly from the olivine. This process can be considered as Ostwald ripening driven by the reduction in surface free energy that results from grain growth. Similar fronts have been reported in naturally occurring examples of serpentine formed from direct alteration of olivine (e.g., Cressey and Zussman, 1976; Hanowski, 1998).

Under the conditions of our experiments (low P, low T), chrysotile would be expected to be the stable alteration product of olivine (Chernosky et al., 1988). However, the absence of fibrous or concentric textures in our serpentines indicates that chrysotile is absent and lizardite is dominant. We interpret this observation as indicating that olivine has been replaced by metastable lizardite, the serpentine polymorph which is regarded as being stable at low temperatures, but higher pressures than chrysotile (Chernosky et al., 1988). This behavior is consistent with studies of terrestrial serpentinization (Moody, 1976; O'Hanley et al., 1989), in which olivine is replaced by lizardite. Although the temperatures of serpentinization are somewhat higher than in our experiments, lizardite is also considered to be a metastable reaction product, stabilized by the close topotactic relationship between the two phases (Moody, 1976). In naturally occurring serpentinites, the lizardite is often subsequently replaced by antigorite (Wicks and Plant, 1979). We do not see any evidence of such a transformation in our experiments, probably due to the fact that stabilization of antigorite requires higher pressures and higher temperatures than our experimental conditions. In addition, it is well-recognized that antigorite is extremely difficult to synthesize experimentally, due to formation of both lizardite and chrysotile that persist metastably for long periods of time (Chernosky et al., 1988).

As noted earlier, the recrystallization of fine-grained serpentine to coarser-grained, platy crystallites has clearly occurred in some experiments (e.g., Fig. 5B). If the lizardite is indeed metastable, it might be expected that this recrystallization process should also have involved the transformation of metastable lizardite to chrysotile, the serpentine polymorph that is likely to be stable at the low temperatures and pressures of our experiments. However, this has clearly not occurred. Instead, the fine-grained lizardite has simply increased in grain size at the recrystallization front. One possible explanation is that the high Al and Fe contents of the lizardite have resulted in an expanded stability field such that it is actually stable at lower pressures than would normally be expected. The incorporation of Fe^{3+} or Al^{3+} by a coupled substitution with Mg and Si could expand the stability field of lizardite because it reduces the misfit between the tetrahedral and octahedral sheets. In addition, according to Wicks and O'Hanley (1988), the composition of lizardite is controlled largely by the bulk composition of the rock, rather than crystal chemical controls. In this respect, the high Fe content of Allende matrix compared with terrestrial ultramafic rocks may well be the major controlling factor in establishing the high Fe contents of the lizardites.

3.2.2. Two-step mechanism

In addition to the direct transformation of olivine to interlayered serpentine and saponite, we have evidence that phyllosilicates form in a two-stage process that involves an amorphous SiO_2-rich intermediate phase. The phyllosilicate and Fe-(hydro)oxide phases that are produced by this second alteration mechanism do not display a direct spatial association, or a crystallographic orientation relationship, with the altering olivine. Rather, we propose that olivine undergoes dissolution according to the equation

$$(Fe_{0.5}Mg_{0.5})_2SiO_4 + 4H^+ = Fe^{2+} + Mg^{2+} + (SiO)_2(aq) + 2H_2O$$

The protons for this reaction are supplied both by dissociation of water (Jenny, 1950)

$$H_2O \rightarrow H^+ + OH^-$$

and by dissolved CO_2 that generates protons according to the equation (Nahon, 1991)

$$CO_2 + H_2O \rightarrow H_2CO_3 \rightarrow H^+ + HCO_3^-$$

Hydrolysis reactions consume H^+ because the hydrogen or hydronium ions displace the cations at the surface of the altering mineral (Nahon, 1991). Thus, as hydrolysis of olivine progresses, the pH of the alteration environment rises and the activities of SiO_2, Mg^{2+}, and Fe^{2+} also increase. Eventually, the fluid will become saturated with respect to silica and will result in the precipitation of a silica-rich phase. We interpret the amorphous SiO_2-rich material that we observe by TEM along the olivine grain boundaries and in the interstices between olivine grains as being the product of such a reaction. In addition, as can be seen in Fig. 9A, an increase of the pH of the system causes Mg^{2+} to be stabilized as a crystalline phase rather than as an aqueous species, forming serpentine and saponite by the schematic reaction

$$Mg^{2+} + Fe^{2+}/Fe^{3+} + SiO_2(s) + H_2O = \text{serpentine} + \text{saponite}$$

These phyllosilicates nucleate and grow in random orientations within the amorphous silica-rich phase (Fig. 5C). Early in the alteration process (i.e., in the sample heated at 200 °C for 30 days at an initial water/rock ratio of 1:1), nanocrystalline phyllosilicates form that are only 2–3 unit cells wide and a few nm long. As alteration increases, and also as a result of thermal activation of crystal growth, these phyllosilicates become well crystallized with curved and wavy morphologies. In the sample heated at 200 °C for 90 days at an initial water/rock ratio of 9:1, individual crystals many 100 s of nm long and up to 20 or 30 unit cells wide form anastamosing complexes over μm-scale distances.

3.3. Origin of interlayering of saponite and serpentine

In our samples heated to 200 °C for 30 days at an initial water/rock ratio of 1:1, and for 90 days at an initial water/rock ratio of 9:1, we observe two phyllosilicate phases, serpentine and saponite, intimately intergrown with one another. Local fluctuations of the activities of silica, Mg, Al, and Fe control the relative stabilities of phyllosilicate phases. Fig. 8 shows the effects of changes in the activities of SiO_2(aq), Mg^{2+}, and H^+ on the stabilities of some relevant Mg-bearing phases and provides some useful insights into the possible origin of the interlayering. This figure is not intended to be representative of what has occurred in our experimental samples, as it does not take into account all the possible phases or all the major cations. Rather, it illustrates the sensitivity of phyllosilicate phases to local changes in the activity of the ions of interest. As olivine is altered in our samples, SiO_2, along with all the octahedral cations, is released into the interstices between altering

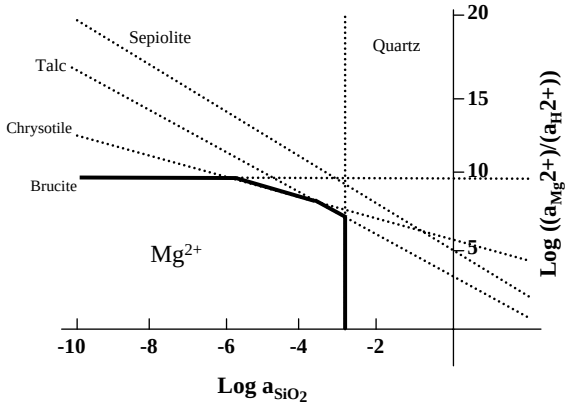

Fig. 8. Activity–activity diagram showing the relative stabilities of Mg-bearing phases at 200 °C as a function of the activity of Mg and SiO_2 as well as pH.

grains. Once the pH and the activities of silica and of the cations reach a critical level, phyllosilicate phases begin to crystallize. The specific phyllosilicate phase that forms depends to a large extent on the local activity of silica. Saponite is stable at higher silica activities than serpentine. Therefore, when silica is being released from the olivine and local silica levels are elevated, saponite is the more stable product phase. As saponite nucleates and grows it incorporates silica, causing a local decrease in silica activity that results in the stabilization of serpentine. Serpentine will continue to nucleate and grow until the silica activity in its immediate surroundings becomes high enough to once again favor the growth of saponite.

The serpentines observed in the 200 °C, 90 days, 9:1 sample are relatively Al-rich, with Al contents as high as 8.4 wt% (Table 3). This is far higher than can be accounted for by isochemical alteration of the matrix olivine which has an average Al_2O_3 content of only 0.36 wt% (Brearley, unpublished data). Alteration of aluminous phases such as nepheline and sodalite is probably the most likely source of Al in Allende matrix (Krot et al., 1995). Alternatively, melilite ($(Ca, Na)_2 (Al, Mg) (Si, Al)_2 O_7$) in CAIs could be an important source of Al, given that melilite in Allende CAIs contains between 10.76 and 35.02 wt% Al_2O_3 and is notably susceptible to aqueous alteration (Krot et al., 1995; McGuire and Hashimoto, 1989).

3.4. Mass transport and source phases

In addition to the direct evidence of alteration of matrix olivines to serpentine and Fe-(hydro)oxides in the interior of the samples, a number of secondary phases occur on the exteriors of the cubes. These phases include calcium sulfate, calcium carbonate, and Fe-(hydro)oxides. In this section, we examine the possible sources of the species that constitute these phases (Ca^{2+}, Mg^{2+}, Fe^{2+}/Fe^{3+}, Al^{3+}, HCO_3^-, SO_4^{2-}, and SiO_2) from direct observations, and from a consideration of the relative alteration susceptibilities of the different precursor phases in Allende. We also consider some possible alteration reactions for the primary phases.

3.4.1. Sulfate and carbonate formation

The widespread presence of $CaSO_4$ and $CaCO_3$ on the exterior of the altered samples attests to the high mobility of Ca during hydrous alteration. Although alteration of a Ca-rich phase might be the source of Ca for the sulfate and carbonate phases, a simple mass balance calculation shows that matrix olivine alteration could account for some of the Ca required. We assume that the matrix of Allende accounts for 38.4 vol % of the meteorite (McSween, 1977), and of that volume 80% is fayalitic olivine with an average composition of Fa_{50} (Scott et al., 1988). This fine-grained fayalitic olivine has an average CaO content of 0.2 wt% (Scott et al., 1988; Zolensky et al., 1993; Brearley, unpublished data). The hydrolysis of 1 mol olivine can be represented by the following equation:

$$(Fe_{0.499}Mg_{0.499}Ca_{0.002})_2SiO_4 + 4H^+ = 0.998Fe^{2+} + 0.998Mg^{2+} + 0.004Ca^{2+} + SiO_2(aq) + 2H_2O$$

A calculation based on the approximate morphology, size, and abundance of Ca-bearing sulfates and carbonates precipitated on the surface of a representative sample (heated at 200 °C for 60 days) shows that an average of 1×10^{-4} g of Ca is required to form these phases. If ~40 to 45 mol% of the matrix olivine in a sample was altered, it would release enough Ca to account for all the secondary Ca-bearing phases observed. We do not observe such extensive alteration of olivine in any of our experiments, so some additional source of Ca such as melilite, which is clearly undergoing alteration in our experiments, is probably also a major source of Ca. A mass balance calculation shows that if a CAI occupied 1 vol % of a sample and contained 30 vol % melilite (an upper limit from Wark (1987)), the melilite would only have to be altered ~14% to account for all the calcium in secondary phases on the surface of the sample. However, our SEM observations indicate that melilite alteration is not so advanced and melilite is unlikely to be the only source of Ca. Numerous other highly calcic phases present in Allende matrix including andradite, wollastonite, kirschteinite, Ca-phosphate, and clinopyroxene (Krot et al., 1998) may also contribute to the calcium balance. We have no direct evidence that these phases are undergoing alteration in our experiments and none of these phases is known to be particularly susceptible to aqueous alteration. However, it is clear that even incipient alteration of these phases could significantly affect the amount of Ca^{2+} available to form carbonates and sulfates.

No sulfates or carbonates have ever been identified occurring naturally in Allende, so the source of sulfate and carbonate ions is clearly not dissolution of preexisting phases. The most plausible source of sulfate cations is the oxidation of sulfides such as pyrrhotite and pentlandite that occur in both the matrix and chondrules in Allende (McSween, 1977; Zolensky et al., 1993). Under oxidizing conditions pyrrhotite alters according to the reaction

$$Fe_{.875}S + 0.125H_2O + 1.938O_2 = 0.25H^+ + 0.875Fe^{2+} + SO_4^{2-}$$

Pentlandite also alters to metal ions, sulfate and protons. One plausible reaction given by Govett et al., 1976 for acid mine drainage is

$$(Fe, Ni)_9S_8 + 32H_2O = 9(Fe, Ni)^{2+} + 8SO_4^{2-} + 64H^+ + 66e^-$$

Although the oxidation of both these sulfide phases releases iron from the sulfide structure, the iron does not enter the fluid phase, but rather is oxidized to its insoluble ferric form and remains closely associated with the altering sulfide grain. This is clearly the case in our experiments as indicated by the presence of secondary Fe-(hydro)oxides on the surfaces of exposed sulfide grains. Both these oxidation reactions produce significant amounts of protons that are required for hydrolysis of olivine, so it is plausible that the oxidation of sulfides in the experiments contributes to the alteration of the matrix olivine. In addition, the sulfate ions produced by the alteration of sulfides are transported in solution to the surface of the sample where they precipitate primarily as $CaSO_4$ and rarely as $MgSO_4$.

Formation of carbonate must require oxidation of indigenous carbon. Allende has a bulk carbon content of 0.25 wt% (Jarosewich et al., 1987), most of which exists as poorly graphitized carbon (PGC) that is homogeneously distributed throughout the matrix (Smith and Buseck, 1981; Brearley, 1999). Oxidation of graphitic carbon in the presence of water may be represented by the reaction

$$\text{graphite} + O_2 + H_2O \rightarrow H^+ + HCO_3^-$$

The equilibrium constant (K) for this reaction at 200 °C is $10^{38.46}$ (calculated using Geochemist's Workbench 3.0). At the pH of the reaction environment (7–8), the bicarbonate ion is the dominant species in solution. Therefore, it is reasonable to assume that this reaction is proceeding to the right, and that any precipitation of carbonate phases will only increase the oxidation of graphite. A mass balance calculation that assumes a carbon content of 0.25 wt% shows that only 0.002% of the carbon needs to be liberated from poorly graphitized carbon in order to supply all the carbon now sequestered in the secondary carbonate phases.

Direct evidence that oxidation of graphitic carbon is an important process in these experiments comes from our TEM observations. Poorly graphitized carbon (PGC) is commonly observed by TEM as inclusions in unaltered olivine grains. However, where significant replacement of the matrix olivine by phyllosilicates has occurred, we did not detect any PGC. We interpret this observation as indicating that as soon as inclusions of poorly graphitized carbon are exposed by alteration of olivine, they undergo oxidation and hence are the most likely candidate for the source of carbon for HCO_3^- ions.

3.5. Fe oxide and oxyhydroxide formation

Fe oxides and oxyhydroxides form by two distinct types of reactions in the experiments, one involving the oxidation of sulfides (see above) and a second involving the oxidation/hydrolysis of FeO-rich matrix olivine. Ferrous iron that is released during dissolution of sulfide phases appears to be very quickly oxidized in situ to ferric iron, which is insoluble and relatively immobile in the experimental system. This mechanism is indicated by the formation of secondary Fe-(hydro)oxide phases closely associated with altering Fe, Ni sulfides (Fig. 2D).

When Fe^{2+} is released during the alteration of matrix olivine, it is oxidized to insoluble Fe^{3+} and is precipitated immediately at the reaction interface to form a cellular intergrowth with the phyllosilicate phases (Fig. 3C). This relative immobility and close association of Fe-(hydro)oxide phases with parent olivine grains has been reported in terrestrial serpentinization and weathering (Eggleton, 1984; Smith et al., 1987; Banfield et al., 1990; Nahon, 1991).

3.6. Carbonate and sulfate precipitation

Given that oxidation and hydration of the matrix phases discussed in the previous section are producing significant amounts of Ca^{2+}, Mg^{2+}, SO_4^{2-}, and HCO_3^-, several questions arise concerning the relative proportions and stabilities of Ca- and Mg-sulfates, and Ca-carbonates. In all our experiments, Ca-bearing phases ($CaSO_4$ and $CaCO_3$) are significantly more abundant than the Mg-bearing sulfates ($MgSO_4$), despite the extensive alteration of olivine as a major source of Mg^{2+} ions. Both $MgSO_4$ and $MgCO_3$ are stable at the temperatures of the experiments, so if both Ca^{2+} and Mg^{2+} were present in the fluid phase it would be expected that these phases would precipitate along with the sulfates and carbonates of calcium.

Fig. 9 shows a series of activity diagrams calculated at 200 °C using Geochemist's Workbench. Fig. 9A shows the relative stabilities of Mg-bearing species and solid phases when SiO_2(aq) is the only other dissolved species in the model solution. At a pH of ~7 to 8 (the pH of our reaction environment), antigorite is stable at $\log a_{Mg^{2+}}$ as low as ~−7 to −5. Fig. 9B is a similar diagram, plotted for Ca under the same model conditions. There is no analogous stable phyllosilicate phase stable in the Ca^{2+} diagram; instead the aqueous ion is stable to relatively high Ca^{2+} activities (almost 1 at pH ~7). We interpret these relative stabilities to indicate that when Mg^{2+} is released from the olivine structure, the activity of Mg^{2+} at which antigorite is stabilized is soon reached and Mg^{2+} is sequestered into the serpentine structure. On the other hand, the solubility of Ca^{2+} is much higher and it enters the fluid phase and is mobilized.

The competition between sulfate and carbonate precipitation is simply related to the relative concentrations of HCO_3^- and SO_4^{2-} ions in solution as illustrated in Fig. 10. Fig. 10A shows the calculated relative stabilities of carbonate and sulfate at 200 °C, with both HCO_3^- and SO_4^{2-} activities set at 10^{-3}. At these conditions, there are large stability fields for both calcite and anhydrite. As the activity of HCO_3^- is incrementally lowered to 10^{-4}, 10^{-5}, and 10^{-6} (Figs. 10B–D), the calcite stability field contracts and moves to higher pHs until, at $HCO_3^- = 10^{-5}$, calcite is no longer stable at the experimental pH of 8, and at $HCO_3^- = 10^{-6}$ the stability field of calcite disappears altogether. A similar effect is observed if the activity of the SO_4^{2-} ion is increased while the activity of HCO_3^- remains constant. Fig. 10E shows the stability fields of calcite and anhydrite at $HCO_3^- = 10^{-3}$ and $SO_4^{2-} = 1$. It is clear that the relative activities of the sulfate and bicarbonate ions control the stabilities of $CaSO_4$ and $CaCO_3$.

Differences in fluid HCO_3^- and SO_4^{2-} activities between samples may be caused by variations in the modal abundance of sulfides in the matrix of the experimental samples. In some experimental samples, relatively high abundances of pyrrhotite and pentlandite may result in higher fluid SO_4^{2-} activities, resulting in the stabilization of sulfate rather than carbonate.

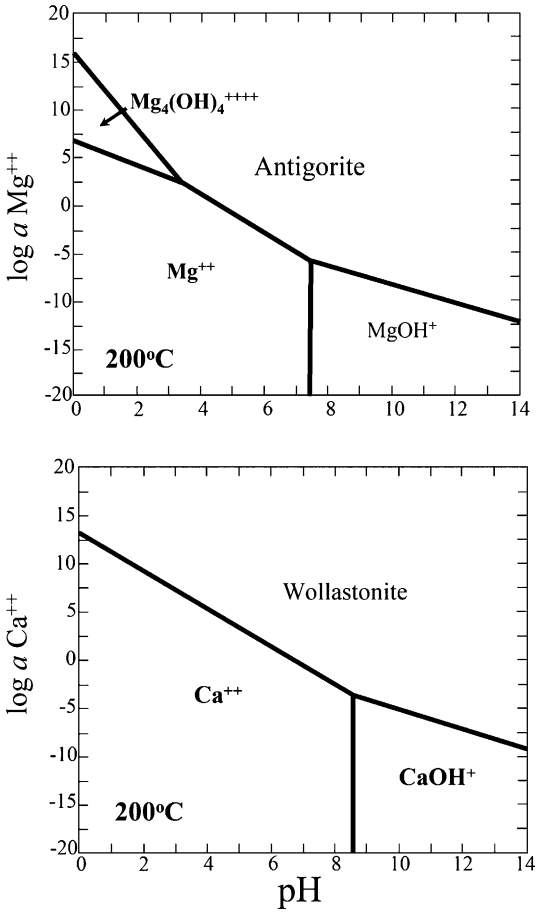

Fig. 9. (A) Activity–activity diagram showing the stability relationships between Mg-bearing phases in the presence of SiO_2 as a function of pH and Mg^{2+} activity at 200 °C. (B) Activity–activity diagram showing the stability relationships between Ca-bearing phases in the presence of SiO_2 as a function of pH and Ca^{2+} activity at 200 °C.

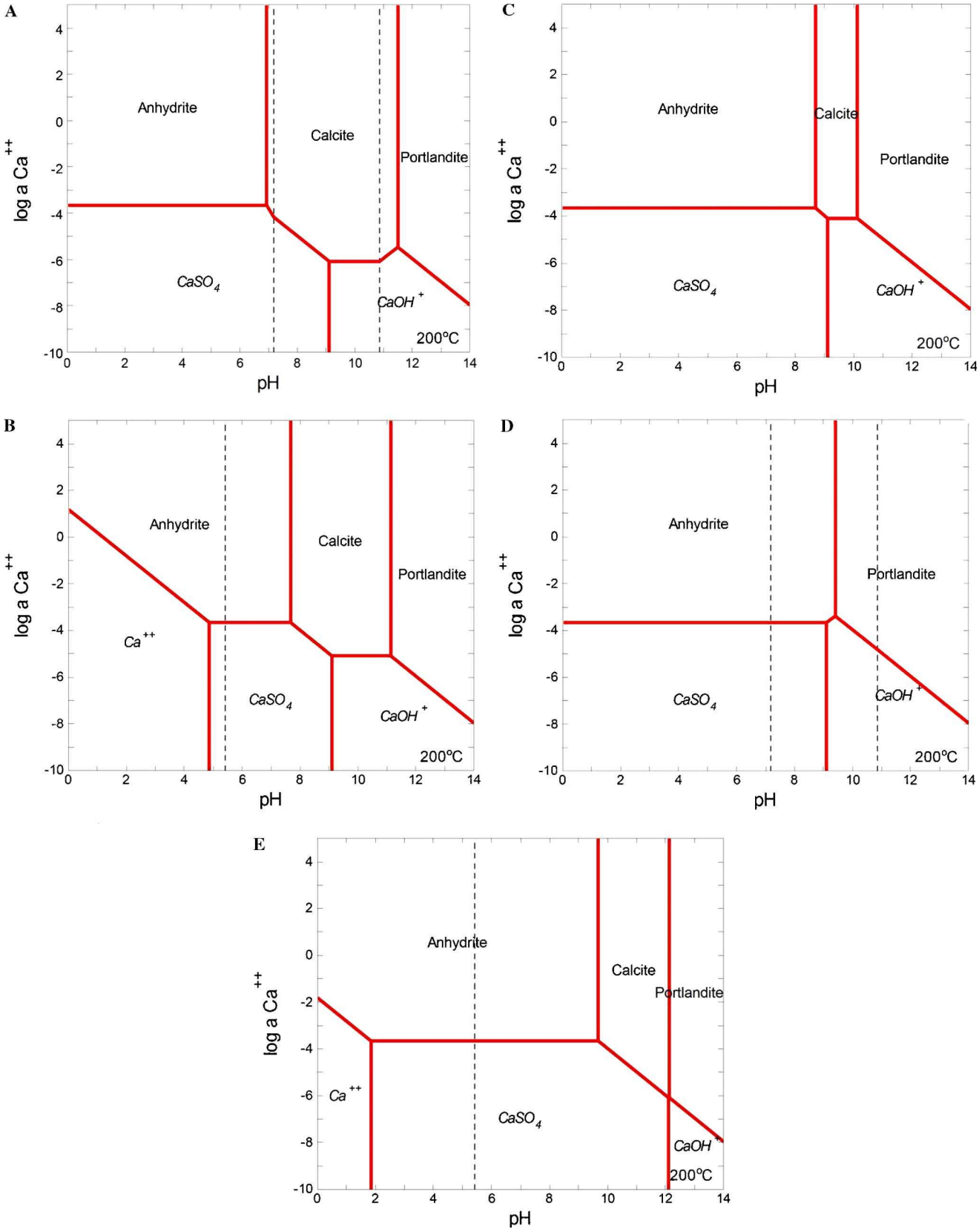

Fig. 10. Activity–activity diagrams showing the stability of Ca-bearing phases as a function of pH and Ca^{2+} activity at 200 °C with variable concentrations of SO_4^{2-} and HCO_3^- ions. (A) $\log[SO_4^{2-}] = -3$, $\log[HCO_3^-] = -3$. (B) $\log[SO_4^{2-}] = -3$, $\log[HCO_3^-] = -4$. (C) $\log[SO_4^{2-}] = -3$, $\log[HCO_3^-] = -5$. (D) $\log[SO_4^{2-}] = -3$, $\log[HCO_3^-] = -6$, (E) $\log[SO_4^{2-}] = 0$, and $\log[HCO_3^-] = -3$.

In some samples, both $CaSO_4$ and $CaCO_3$ are present and, in most cases, textural evidence indicates that the carbonate precipitates first and the sulfate second (Fig. 1E). This relationship can be explained using the calculated activity diagrams shown in Fig. 10. If the activities of sulfate and carbonate ions in the fluids are approximately equal, calcite is stable (Fig. 10A). If calcite precipitates, depleting the fluid in HCO_3^-, the stability field of calcite contracts and moves to higher pHs (Figs. 10B and C). Thus, in our experiments precipitation of the $CaCO_3$ phase depletes fluid HCO_3^- levels, a change in conditions which stabilizes $CaSO_4$ (at pH 8) and it precipitates after the carbonate. This process requires that there is a kinetic control on the formation of bicarbonate ions, i.e., that the oxidation of graphitic material is rate-controlling and is slower than sulfate-forming reactions. Given the high reactivity of sulfides in oxidizing fluids and the refractory nature of graphitic carbon, it seems likely that bicarbonate formation by oxidation of graphite would be the slower process.

3.7. Implications for the aqueous alteration of carbonaceous chondrites

These experiments are not intended to replicate aqueous alteration in any specific carbonaceous chondrite group, but were carried out to gain general insights into the alteration behavior of plausible chondritic mineral assemblages under highly oxidizing conditions, over a range of temperatures. The temperature range of 100–200 °C extends from the conditions estimated for alteration of the CI chondrites (e.g., Clayton and Mayeda, 1984; Zolensky et al., 1993), to temperatures higher than were probably experienced by most carbonaceous chondrites. Nevertheless, these higher temperature experiments provide useful data on the kinetics of alteration reactions and possible changes in alteration mechanism that can occur as a function of temperature. In addition, they provide some useful insights into the very earliest stages of aqueous alteration that are not commonly observed in carbonaceous chondrites.

The alteration phases formed in our experiments, principally serpentine, saponite, Fe-(hydro)oxides, $CaSO_4$, and $CaCO_3$ are all phases that occur in altered carbonaceous chondrites. This assemblage is closest to that observed in the CI chondrites, which contain intergrown serpentine and saponite, carbonates and sulfates as well as iron oxides (predominantly magnetite). This is perhaps to be expected given that the CI chondrites appear to have been altered under relatively oxidizing conditions (Zolensky et al., 1993), similar to those in our experiments. In comparison with our experiments, however, the CI chondrites are essentially completely altered and have mineral compositions that differ in a number of respects from our experiments. The carbonates in CI chondrites are much more complex and diverse than in our experiments and include dolomite, breunnerite, and calcite. These differences may be a reflection of the more advanced degree of alteration in the CIs and indicate that carbonate assemblages evolve progressively as alteration becomes more advanced.

Our lowest temperature experiments in which very limited aqueous alteration has occurred provide an interesting comparison with carbonaceous chondrites that have experienced incipient to minor aqueous alteration. These include members of the CV and CO carbonaceous chondrite groups, but we focus here, for brevity on the CV chondrites. The CV chondrites show a range of degrees of aqueous alteration from incipient in Vigarano and Mokoia to extensive in Bali and Kaba. In Kaba and Bali, the alteration of the matrix has resulted in the formation of fibrous saponite (Keller and Buseck, 1990; Keller et al., 1994) that appears to have replaced matrix olivine. In most cases, however, development of the saponite has occurred in the interstices between the olivine grains, filling in porosity. Keller and Buseck (1990) and Keller et al. (1994) interpreted their observations as being indicative of alteration at low temperatures (<100 °C), based on the presence of saponite rather than serpentine as an alteration product. Our experiments indicate that the mechanism of FeO-rich ($\sim Fa_{50}$) olivine alteration is strongly temperature dependent and may be useful in constraining alteration conditions in these CV chondrites. Above ~150 °C in our experiments, alteration is dominated by crystallographically controlled replacement of FeO-rich olivine by serpentine and saponite intergrowths, but at lower temperatures (150 °C) alteration occurs predominantly by dissolution of olivine followed by precipitation of interstitial amorphous silica-rich material. It is noteworthy that Keller and Buseck (1990) and Keller et al. (1994) found only limited evidence of crystallographic orientation relationships between matrix olivines and their alteration products, saponite and serpentine in Kaba and Bali. This suggests that the phyllosilicates in these two meteorites formed dominantly by the dissolution/reprecipitation mechanism, again consistent with alteration at temperatures around or below 150 °C. We have not observed relatively well-crystallized fibrous saponite in our lowest temperature experiments, probably because these experiments represent only the earliest stage of olivine alteration. It is likely that Bali and Kaba experienced alteration for much more extended periods of time than our experiments and that the abundant fibrous saponite is due to thermally activated, progressive recrystallization of an intermediate, amorphous silica-rich phase.

Although there are clearly similarities between the phyllosilicates in these CV chondrites and those formed in our experiments, the absence of carbonates and sulfates in these meteorites is striking, given their abundance in our experiments. Why Ca, in particular, was not mobilized and precipitated as carbonate is not clear at this point, given that in other altered meteorites, such as CIs, CMs, CRs, and some UOCs, carbonate formation is ubiquitous. Redox conditions in our experiments appear to have been similar to those in CV chondrites as indicated by the common presence of magnetite and/or ferrihydrite in altered

CV chondrites (Tomeoka and Buseck, 1990; Keller and Buseck, 1990; Keller et al., 1994; Lee et al., 1996). On these grounds, oxidation of at least some component of organic material to form carbonate would be expected, but has clearly not occurred.

Mineralogically our experimental samples resemble CR chondrites as indicated by the presence of saponite, serpentine, and carbonates (e.g., Zolensky et al., 1993; Weisberg et al., 1993). However, in detail there are important differences. Recent TEM studies of several CR chondrites (Abreu and Brearley, 2004, 2005a,b) show that the main phyllosilicates are interlayered serpentine and saponite, as in our experimental samples. However, the grain size of the CR phyllosilicates is significantly less than in our 200 °C experiments, supporting the view that alteration of this group occurred at lower temperatures (e.g., ~50–150 °C; Zolensky et al., 1993). However, contrary to the observations of Zolensky et al. (1993) on CR chondrite matrices, Abreu and Brearley (2004, 2005a,b) found that olivine is essentially absent. The formation of phyllosilicates in the matrices CR chondrites does not appear to have involved the alteration of olivine, unlike our experiments.

Our experiments are notably different from the alteration experienced by the CM chondrites. Serpentine is the dominant phyllosilicate phase produced during alteration of these meteorites not saponite/serpentine. In addition, tochilinite intergrown with cronstedtite is perhaps the most diagnostic characteristic of alteration for CM chondrites (Brearley and Jones, 1998), and is not found in any other chondrite group or in our experimental alteration assemblage. We interpret these differences as indicating that alteration of the CM chondrites occurred under less oxidizing conditions than our experiments, also consistent with the absence of magnetite in most CMs (Zolensky et al., 1989; Rosenberg et al., 2001). It is possible that other variables such as water/rock ratio, pH, and temperature may have a second order influence on the mineral assemblages, but in the case of CMs relatively reducing conditions appears to have been the major factor in stabilizing tochilinite (e.g., Browning and Bourcier, 1996).

One of the most significant findings of our experiments concerns the rates of alteration of chondritic materials and the implications that this has for the timescales of alteration on asteroidal parent bodies. It is clear that interaction of carbonaceous chondrites with liquid water, even for extremely short periods of time, geologically speaking, will result in a mineralogical signature of alteration. Our limited experimental results at 100 °C, show that even after just 6 months, evidence of oxidation, and formation of carbonates and sulfates is apparent. However, development of phyllosilicates at these temperatures appears to be much more sluggish and is clearly strongly temperature dependent. Our experiments do not allow us to extract quantitative kinetic data for the formation of phyllosilicates at the lowest temperatures of alteration estimated for carbonaceous chondrites. However, over the temperature range 150–200 °C, phyllosilicate formation occurs on timescales of days to weeks. Our TEM data indicate that approximately the same degree of phyllosilicate formation, i.e., olivine hydration occurs in ~15 days at 200 °C as is apparent at 150 °C after 60 days, allowing us to make a very crude extrapolation of reaction rates to lower temperatures. An exponential fit to these data indicate that at temperatures of ~25 °C incipient formation could have occurred on a timescale of ~5000–10,000 years. This extrapolation may be at least two orders of magnitude in error, but illustrates that evidence of early phyllosilicate formation can reasonably expected in time periods on the order of 100s to 1000s of years. This result is consistent with dissolution rates calculated by Lasaga (1984) for a range of silicate minerals, that suggest a 1 mm crystal of olivine would completely dissolve within ~600,000 years.

4. Conclusions

The anhydrous mineral assemblages in Allende are clearly highly susceptible to aqueous alteration under oxidizing conditions between 100 and 200 °C. At the lowest temperatures, evidence of incipient alteration is apparent in a matter of weeks, compared with days at 200 °C. In all samples, mobilization and reprecipitation of soluble elements is extensive as indicated by the precipitation of calcium carbonate and calcium sulfate on the surfaces of the altering samples. Oxidation of surface olivine to a red-brown coloration is also apparent. In the interior of the sample, alteration has occurred predominantly in the fine-grained matrix, where the primary alteration is the oxidation and hydration of fine-grained fayalitic olivine. Additional key reactions appear to be oxidation of matrix sulfides and of poorly graphitized carbon.

Matrix olivine grains alter to interlayered serpentine and saponite as well as Fe-(hydro)oxides via two distinct mechanisms, that appear to be a function of temperature. At temperatures above ~150 °C, olivine alteration occurs by the formation of crystallographically oriented phyllosilicates that nucleate on the surface of the olivine grains, with the orientation relationship $c_{serp/sap}//a_{ol}$. The Fe-(hydro)oxide phase in this case is intimately intergrown with the serpentine and saponite. For the second mechanism that occurs in all the experiments, matrix olivine undergoes dissolution and reprecipitation to form an amorphous silica phase that then recrystallizes to serpentine. The serpentine grains are randomly oriented, and have grown independently of any crystallographic control by the parent olivine. The Fe-(hydro)oxides form large, distinct precipitate complexes rather than being intergrown with the serpentine.

In general, the alteration assemblages observed in our experiments are broadly comparable with secondary phases that are present in altered carbonaceous chondrites. This suggests that the temperatures and water/rock ratios investigated in our experiments are similar to those experienced by the parent asteroids of these chondrites, although our

experimental results are not an exact match for any specific chondrite. Detailed comparisons with the alteration assemblages in CI, CM, CV, and CR chondrites, indicate that our data are most comparable with alteration observed in CI and CR chondrites and, to a lesser extent, some CV chondrites. The differences between the natural assemblages and our experiments appear to be reasonably explained by higher temperatures of alteration and shorter reaction times in our experiments, and provide independent support for alteration temperatures <100 °C for these chondrites.

Finally, our data provide some constraints on the timescale of alteration for carbonaceous chondrites. Assuming an exponential dependence of reaction rates on temperature, and provided that water is continually present during alteration on chondrite parent bodies, our results suggest that incipient alteration would occur on timescales of 100s to 1000s of years at 25 °C. For alteration as extensive as is observed in CI and CM chondrites, timescales for alteration within hundreds of thousands to 1–2 million years is probably reasonable and is consistent with Mn–Cr ages for the oldest ages of carbonate formation in CM chondrites (Yamato 791198) of ~4.5 million years after CAI formation (Brearley et al., 2001; Brearley and Hutcheon, 2002).

Acknowledgments

The very thorough reviews of Dr. Kazu Tomeoka, Dr. Mike Zolensky, and an anonymous reviewer are gratefully acknowledged and helped improve the manuscript significantly. We are also grateful to Mike Spilde and Tom Servilla for technical assistance, and James Papike, Laura Crossey, Rhian Jones, and Paul Burger for many helpful discussions. Electron microscopy was performed in the Electron Microbeam Analysis Facility, Department of Earth and Planetary Sciences and Institute of Meteoritics, University of New Mexico, a facility supported by NSF, through the NSF National Nanosciences Infrastructure Network (NNIN), NASA and the State of New Mexico. This research was supported by NASA Origins of Solar System Grants NAG5-4619 and NAG5-11862 to Adrian Brearley (PI).

Associate editor: Alexander N. Krot

References

Abreu, N.M., Brearley, A.J., 2004. Characterization of matrix in the EET92042 CR2 carbonaceous chondrite: insights into textural and mineralogical heterogeneity (abstract). *Meteor. Planet. Sci.* **39**, 178A (abstract).

Abreu, N.M., Brearley, A.J., 2005. HRTEM and EFTEM studies of phyllosilicate-organic matter associations in matrix and dark inclusions in the EET92042 CR2 carbonaceous chondrite. Lunar Planet. Sci. XXXVI, Lunar Planet. Inst., Houston, Houston #1744 (abstract).

Banfield, J.F., Veblen, D.R., Jones, B.F., 1990. Transmission electron microscopy of subsolidus oxidation and weathering of olivine. *Contrib. Miner. Petrol.* **106**, 110–123.

Bass, M.N., 1971. Montmorillonite and serpentine in Orgueil meteorite. *Geochim. Cosmochim. Acta* **35**, 139–147.

Boström, K., Fredriksson, K., 1966. Surface conditions of the Orgueil parent meteorite body as indicated by mineral associations. Smithson. Misc. Collect. 151, no. 3, 39 pp.

Brearley, A.J., 1995. Aqueous alteration and brecciation in Bells, an unusual, saponite-bearing, CM chondrite. *Geochim. Cosmochim. Acta* **59**, 2291–2317.

Brearley, A.J., 1997. Disordered biopyriboles, amphibole, and talc in the Allende meteorite: products of nebular or parent body aqueous alteration? *Science* **276**, 1103–1105.

Brearley, A.J., 1999. Origin of graphitic carbon and pentlandite in matrix olivines in the Allende meteorite. *Science* **285**, 1380–1382.

Brearley, A.J., 2003. Nebular vs parent body processing of chondritic meteorites. In: Davis, A.M. (Ed.), '*Treatise on Geochemistry*'. In: Holland, H.D., Turekian, K.K. (Eds.), *Cosmochemisty*, Vol. 1. Elsevier, pp. 1–22.

Brearley, A.J., Duke, C.L., 1998. Aqueous alteration of chondritic meteorites: insights from experimental low temperature hydrothermal alteration of Allende (abstract). Lunar Planet. Sci. XXIX, Lunar Planet. Inst., Houston, #1247 (abstract).

Brearley, A.J., Jones, R.H., 1998. Chondritic meteorites. In: Papike, J.J. (Ed.), *Reviews in Mineralogy, Planetary Materials*, vol. 36. Mineralogical Society of America, Washington, DC, p. 398.

Brearley, A.J., Hutcheon, I.D., 2002. Carbonates in the Y791918 CM2 chondrite: zoning and Mn–Cr systematics (abstract). *Meteor. Planet. Sci.* **37**, A23.

Brearley, A.J., Hutcheon, I.D., Browning, L., 2001. Compositional zoning and Mn–Cr systematics in carbonates from the Y791198 CM2 carbonaceous chondrite (abstract). Lunar Planet. Sci. XXXII, Lunar Planet. Inst., Houston, #1458 (abstract).

Browning, L.B., Bourcier, W.L., 1996. Tochilinite: a sensitive indicator of alteration conditions on the CM asteroidal parent body (abstract). Lunar Planet. Sci. XXVII, 171–172. Lunar and Planetary Institute, Houston (abstract).

Chernosky, J.V., Berman, R.G., Bryndzia, L.T., 1988. Stability, phase relations and thermodynamic properties of chlorite and serpentine minerals. In: Bailey, S.W. (Ed.), *Hydrous Phyllosilicates (Exclusive of Micas)*, *Reviews in Mineralogy*, vol. 19. Mineralogical Society of America, Washington, DC, pp. 291–346.

Clayton, R.N., Mayeda, T.K., 1984. The oxygen isotope record in Murchison and other carbonaceous chondrites. *Earth Planet. Sci. Lett.* **67**, 151–161.

Cressey, B.A., Zussman, J., 1976. Electron microscopic studies of serpentinites. *Can. Miner.* **14**, 307–313.

Deer, W.A., Howie, R.A., Zussman, J., 1966. Rock-forming Minerals, vol. 3., Wiley, New York.

DuFresne, E.R., Anders, E., 1962. On the chemical evolution of the carbonaceous chondrites. *Geochim. Cosmochim. Acta* **26**, 1085–1114.

Duke, C.L., Brearley, A.J., 1998. Experimental aqueous alteration of Allende (CV3) (abstract). *Meteor. Planet. Sci.* **33**, A43.

Duke, C.L., Brearley, A.J., 1999. Experimental low temperature aqueous alteration of Allende under reducing conditions. Lunar Planet. Sci. XXXVI, Lunar Planet. Inst., Houston, Houston #1782 (abstract).

Eggleton, R.A., 1984. Formation of iddingsite rims on olivine: a transmission electron microscope study. *Clay Clay Miner.* **32**, 1–11.

Govett, G.J.S., Goodfellow, W.D., Whitehead, R.E.S., 1976. Experimental aqueous dispersion of elements around sulfides. *Econ. Geol.* **71**, 925–940.

Hanowski, N.P., 1998. The aqueous alteration of CM carbonaceous chondrites: petrographic and microchemical constraints. PhD Dissertation. University of New Mexico. pp. 237.

Haar, L., Gallagher, J.S., Kell, G.S., 1984. *NBS/NRC Steam Tables*. Hemisphere Publishing, New York, pp. 320.

Hashimoto, A., Grossman, L., 1987. Alteration of Al-rich inclusions inside ameboid olivine aggregates in the Allende meteorite. *Geochim. Cosmochim. Acta* **51**, 1685–1704.

Jarosewich, E., Clarke Jr., R.S., Barrow, J.N., 1987. The Allende meteorite reference sample. *Smithsonian Contrib. Earth Sci.*, 27.

Jenny, H., 1950. Origin of soils. In: Trask, P.D. (Ed.), *Applied Sedimentation*. Wiley, New York, pp. 41–61.

Jones, C.L., 2000. Aqueous alteration of chondritic meteorites: insights from experimental low temperature hydrothermal alteration of Allende. M.S. Thesis, University of New Mexico, pp. 140.

Keller, L.P., Buseck, P.R., 1990. Aqueous alteration in the Kaba CV3 carbonaceous chondrite. *Geochim. Cosmochim. Acta* **54**, 2113–2120.

Keller, L.P., Buseck, P.R., 1991. Calcic micas in the Allende meteorite: evidence for hydration reactions in the early solar nebula. *Science* **252**, 946–949.

Keller, L.P., Thomas, K.L., Clayton, R.N., Mayeda, T.K., DeHart, J.M., McKay, D.S., 1994. Aqueous alteration of the Bali CV3 chondrite: evidence from mineralogy, mineral chemistry, and oxygen isotopic compositions. *Geochim. Cosmochim. Acta* **58**, 5589–5598.

Kerridge, J.F., 1964. Low-temperature minerals from the fine-grained matrix of some carbonaceous meteorites. *Ann. Natl. Acad. Sci.* **119**, 41–53.

Klein, C., Hurlbut Jr., C.S., 1993. *Manual of Mineralogy*. John Wiley, New York, p. 427.

Klimentidis, R., Mackinnon, I.D.R., 1986. High-resolution imaging of ordered mixed-layer clays. *Clay Clay Miner.* **34**, 155–164.

Kojima, T., Tomeoka, K., 1999. Experimental hydrothermal alteration of the Allende CV3 chondrite under acidic and neutral conditions (abstract). *Meteor. Planet. Sci.* **34**, A67.

Kojima, T., Tomeoka, K., 2000. Transmission electron microscopy of phyllosilicates in experimentally altered Allende: comparison to naturally altered CV3 chondrites (abstract). *Meteor. Planet. Sci.* **35**, A90.

Krot, A.N., Scott, E.R.D., Zolensky, M.F., 1995. Mineralogical and chemical modification of components in CV3 chondrites: nebular or asteroidal processing? *Meteoritics* **30**, 748–775.

Krot, A.N., Petaev, M.I., Scott, E.R.D., Choi, B.-G, Zolensky, M.E., Keil, K., 1998. Progressive alteration in CV3 chondrites: more evidence for asteroidal alteration. *Meteor. Planet. Sci.* **33**, 1065–1085.

Kvasha, L.G., 1948. Investigation of the stony iron meteorite Staroye Boriskino. *Meteoritika* **4**, 83–96.

Lasaga, A.C., 1984. Chemical kinetics of water–rock interactions. *J. Geophys. Res.* **89** (B6), 400–04025.

Lee, M.R., Hutchison, R., Graham, A.L., 1996. Aqueous alteration in the matrix of the Vigarano (CV3) carbonaceous chondrite. *Meteor. Planet. Sci.* **31**, 477–483.

Mason, B., 1960. The origin of meteorites. *J. Geophys. Res.* **65**, 2965–2970.

McGuire, A.V., Hashimoto, A., 1989. Origin of zoned fine-grained inclusions in the Allende meteorite. *Geochim. Cosmochim. Acta* **53**, 1123–1133.

McSween Jr., H.Y., 1977. Petrographic variations among carbonaceous chondrites of the Vigarano type. *Geochim. Cosmochim. Acta* **41**, 1777–1790.

Moody, J.B., 1976. An experimental study of the serpentinization of iron-bearing olivines. *Can. Miner.* **14**, 462–478.

Nagy, B., 1966. Investigation of the Orgueil carbonaceous meteorite. *Geol. Foren. Stockholm Forh.* **88**, 235–272.

Nahon, D.B., 1991. *Introduction to the Petrology of Soils and Chemical Weathering*. John Wiley, New York.

O'Hanley, D.S., Chernosky Jr., J.V., Wicks, F.J., 1989. The stability of lizardite and chrysotile. *Can. Miner.* **207**, 483–493.

Peck, J.A., 1983. Mineralogy and chemistry of CV3 chondrite matrix: Clues to processes in the early nebula. B.S. Thesis, Harvard.

Pisani, F., 1864. Etude chimique et analyse de l'aerolithe d'Orgueil. *Compt. Rend.* **59**, 132–135.

Rosenberg, N.D., Browning, L., Bourcier, W.L., 2001. Modeling aqueous alteration of CM carbonaceous chondrites. *Meteor. Planet. Sci.* **36**, 239–244.

Scott, E.R.D., Barber, D.J., Alexander, C.M., Hutchison, R., Peck, J.A., 1988. Primitive material surviving in chondrites: matrix. In: Kerridge, J.F., Matthews, M.S. (Eds.), Meteorites and the Early Solar System. University of Arizona Press, pp. 718–745.

Smith, K.L., Milnes, A.R., Eggleton, R.A., 1987. Weathering of basalt: formation of iddingsite. *Clay Clay Miner.* **35**, 418–428.

Smith, P.P.K., Buseck, P.R., 1981. Graphitic carbon in the Allende meteorite: a microstructural study. *Science* **212**, 322–324.

Tomeoka, K., Buseck, P.R., 1982a. An unusual layered mineral in chondrules and aggregates of the Allende carbonaceous chondrite. *Nature* **299**, 327–329.

Tomeoka, K., Buseck, P.R., 1982b. Intergrown mica and montmorillonite in the Allende carbonaceous chondrite. *Nature* **299**, 326–327.

Tomeoka, K., Buseck, P.R., 1988. Matrix mineralogy of the Orgueil CI carbonaceous chondrite. *Geochim. Cosmochim. Acta* **52**, 1627–1640.

Tomeoka, K., Buseck, P.R., 1990. Phyllosilicates in the Mokoia CV carbonaceous chondrite: evidence for aqueous alteration in an oxidizing condition. *Geochim. Cosmochim. Acta* **54**, 1745–1754.

Tomeoka, K., Kojima, T., 1995. Experimental aqueous alteration of the Allende CV3 chondrite (abstract). *Meteoritics* **30**, 588–589.

Tomeoka, K., Kojima, T., 1995. Aqueous alteration of the Allende CV3 chondrite: a hydrothermal experiment (abstract). *Antarct. Meteorites* **20**, 251–253.

Toriumi, M., 1989. Grain size distribution of the matrix in the Allende chondrite. *Earth Planet. Sci. Lett.* **92**, 265–273.

Wark, D.A., 1987. Plagioclase-rich inclusions in carbonaceous chondrite meteorites: liquid condensates? *Geochim. Cosmochim. Acta* **51**, 221–242.

Wark, D.A., Lovering, J.F., 1977. Marker events in the early evolution of the solar system: evidence from rims on Ca–Al-rich inclusions from carbonaceous chondrites. In: Proc. Lunar Planet. Sci. Conf. 8th, pp. 95–112.

Weisberg, M.K., Prinz, M., Clayton, R.N., Mayeda, T.K., 1993. The CR (Renazzo-type) carbonaceous chondrite group and its implications. *Geochim. Cosmochim. Acta* **57**, 1567–1586.

Wicks, F.J., Plant, A.G., 1979. Electron-microprobe and X-ray-microbeam studies of serpentine textures. *Can. Miner.* **17**, 785–830.

Wicks, F.J., O'Hanley, D.S., 1988. Serpentine minerals: structures and petrology. In: Bailey, S.W. (Ed.), *Hydrous Phyllosilicates (Exclusive of Micas)*, *Reviews in Mineralogy*, vol. 19. Mineralogical Society of America, Washington, DC, pp. 90–167.

Zolensky, M., McSween, H.Y., Jr., 1988. Aqueous alteration. In: Kerridge, J.F., Matthews, M.S. (Eds.), Meteorites and the Early Solar System. University of Arizona Press, pp. 114–143.

Zolensky, M., Barrett, R., Browning, L., 1993. Mineralogy and composition of matrix and chondrule rims in carbonaceous chondrites. *Geochim. Cosmochim. Acta* **57**, 3123–3148.

Zolensky, M., Bourcier, W.L., Gooding, J.L., 1989. Aqueous alteration on the hydrous asteroids: results of EQ3/6 computer simulations. *Icarus* **78**, 411–425.